

# Pro-efferocytic nanoparticles are specifically taken up by lesional macrophages and prevent atherosclerosis

Alyssa M. Flores<sup>1,9</sup>, Niloufar Hosseini-Nassab<sup>2,9</sup>, Kai-Uwe Jarr<sup>1,9</sup>, Jianqin Ye<sup>1</sup>, Xingjun Zhu<sup>2</sup>, Robert Wirka<sup>3</sup>, Ai Leen Koh<sup>4</sup>, Pavlos Tsantilas<sup>1</sup>, Ying Wang<sup>1</sup>, Vivek Nanda<sup>1</sup>, Yoko Kojima<sup>1</sup>, Yitian Zeng<sup>4</sup>, Mozghan Lotfi<sup>1</sup>, Robert Sinclair<sup>4</sup>, Irving L. Weissman<sup>5</sup>, Erik Ingelsson<sup>3,6</sup>, Bryan Ronain Smith<sup>2,7,8,10\*</sup> and Nicholas J. Leeper<sup>1,3,6,10\*</sup>

**Atherosclerosis is the process that underlies heart attack and stroke. A characteristic feature of the atherosclerotic plaque is the accumulation of apoptotic cells in the necrotic core. Prophagocytic antibody-based therapies are currently being explored to stimulate the phagocytic clearance of apoptotic cells; however, these therapies can cause off-target clearance of healthy tissues, which leads to toxicities such as anaemia. Here we developed a macrophage-specific nanotherapy based on single-walled carbon nanotubes loaded with a chemical inhibitor of the antiphagocytic CD47-SIRP $\alpha$  signalling axis. We demonstrate that these single-walled carbon nanotubes accumulate within the atherosclerotic plaque, reactivate lesional phagocytosis and reduce the plaque burden in atheroprone apolipoprotein-E-deficient mice without compromising safety, and thereby overcome a key translational barrier for this class of drugs. Single-cell RNA sequencing analysis reveals that prophagocytic single-walled carbon nanotubes decrease the expression of inflammatory genes linked to cytokine and chemokine pathways in lesional macrophages, which demonstrates the potential of 'Trojan horse' nanoparticles to prevent atherosclerotic cardiovascular disease.**

The phagocytic clearance of apoptotic cells (ACs) is a routine homeostatic process that protects tissues from exposure to the inflammatory contents of dying cells<sup>1–3</sup>. To remove these cells, the body engages in a process known as efferocytosis ('to take to the grave'). Efferocytosis is a highly conserved process triggered by 'eat me' ligands, which signal to phagocytes to induce engulfment<sup>1</sup>. Conversely, cells may overexpress 'don't eat me' ligands to avoid removal<sup>4</sup>.

By delivering an antiphagocytic signal that enables immune evasion, the upregulation of the 'don't eat me' molecule, CD47, is a major mechanism by which cancers establish and propagate disease<sup>4,5</sup>. We recently discovered that CD47 signalling also has a critical role in atherosclerosis<sup>6</sup>. Atherosclerosis is the process that underlies heart attack and stroke and has remained the leading cause of death in the United States for nearly the past century<sup>7,8</sup>. While pursuing the mechanism by which apoptotic vascular cells escape clearance from the diseased artery, we found that CD47 is markedly upregulated in the atherosclerotic plaque<sup>6</sup>.

CD47 functions as a ligand for the signal regulatory protein- $\alpha$  (SIRP $\alpha$ ) on macrophages<sup>9</sup>. After this interaction, SIRP $\alpha$  activates the Src homology 2 domain-containing phosphatase-1 (SHP-1) to mediate the intracellular signalling that suppresses phagocytic function<sup>10</sup>. This signalling cascade renders diseased vascular cells resistant to removal and promotes plaque expansion. In hyperlipidaemic

mice, CD47-blocking antibodies normalize the defect in efferocytosis, prevent the progression of established lesions, and protect against plaque rupture<sup>6</sup>. However, the antibody-mediated blockade of CD47 also accelerates the off-target removal of certain healthy tissue, which includes the Fc-mediated elimination of red blood cells (RBCs) in the spleen<sup>6,11,12</sup>. The resulting anaemia and reduced oxygen-carrying capacity may exacerbate ischaemia in individuals with atherosclerotic disease, and thus limit the translational potential of the systemic pro-efferocytic therapies currently in development.

To develop a method that more specifically and safely restores impaired efferocytic activity, we precision-engineered nanoparticles (NPs) that interrupt CD47-SIRP $\alpha$  signalling in monocytes and macrophages. The system, termed SWNT-SHP1i, involves a backbone of polyethylene glycol (PEG)-functionalized single-walled carbon nanotubes (SWNTs) loaded with (1) a fluorescent probe Cy5.5 and (2) a small-molecule inhibitor of CD47's downstream effector molecule, SHP-1 (Fig. 1a). PEG-functionalized SWNTs were chosen because of their ultrahigh loading capacity<sup>13</sup>, favourable toxicology<sup>14,15</sup> and ability to accumulate within a specific leukocyte subset, Ly-6C<sup>hi</sup> monocytes (inflammatory monocytes)<sup>16</sup>. The selectivity for this cell type is important, as Ly-6C<sup>hi</sup> monocytes are the primary circulating cells recruited to the diseased artery, where they differentiate into lesional macrophages<sup>17–19</sup>. In addition to regulating

<sup>1</sup>Department of Surgery, Division of Vascular Surgery, Stanford University School of Medicine, Stanford, CA, USA. <sup>2</sup>Department of Radiology, Stanford University School of Medicine, Stanford, CA, USA. <sup>3</sup>Department of Medicine, Division of Cardiovascular Medicine, Stanford University School of Medicine, Stanford, CA, USA. <sup>4</sup>Department of Materials Science and Engineering, Stanford University, Stanford, CA, USA. <sup>5</sup>Stanford Institute for Stem Cell Biology and Regenerative Medicine, Stanford, CA, USA. <sup>6</sup>Stanford Cardiovascular Institute, Stanford, CA, USA. <sup>7</sup>Department of Biomedical Engineering, Michigan State University, East Lansing, MI, USA. <sup>8</sup>Institute for Quantitative Health Science and Engineering, East Lansing, MI, USA. <sup>9</sup>These authors contributed equally: Alyssa M. Flores, Niloufar Hosseini-Nassab, Kai-Uwe Jarr. <sup>10</sup>These authors contributed equally: Bryan Ronain Smith, Nicholas J. Leeper.

\*e-mail: [smit2901@msu.edu](mailto:smit2901@msu.edu); [nleeper@stanford.edu](mailto:nleeper@stanford.edu)

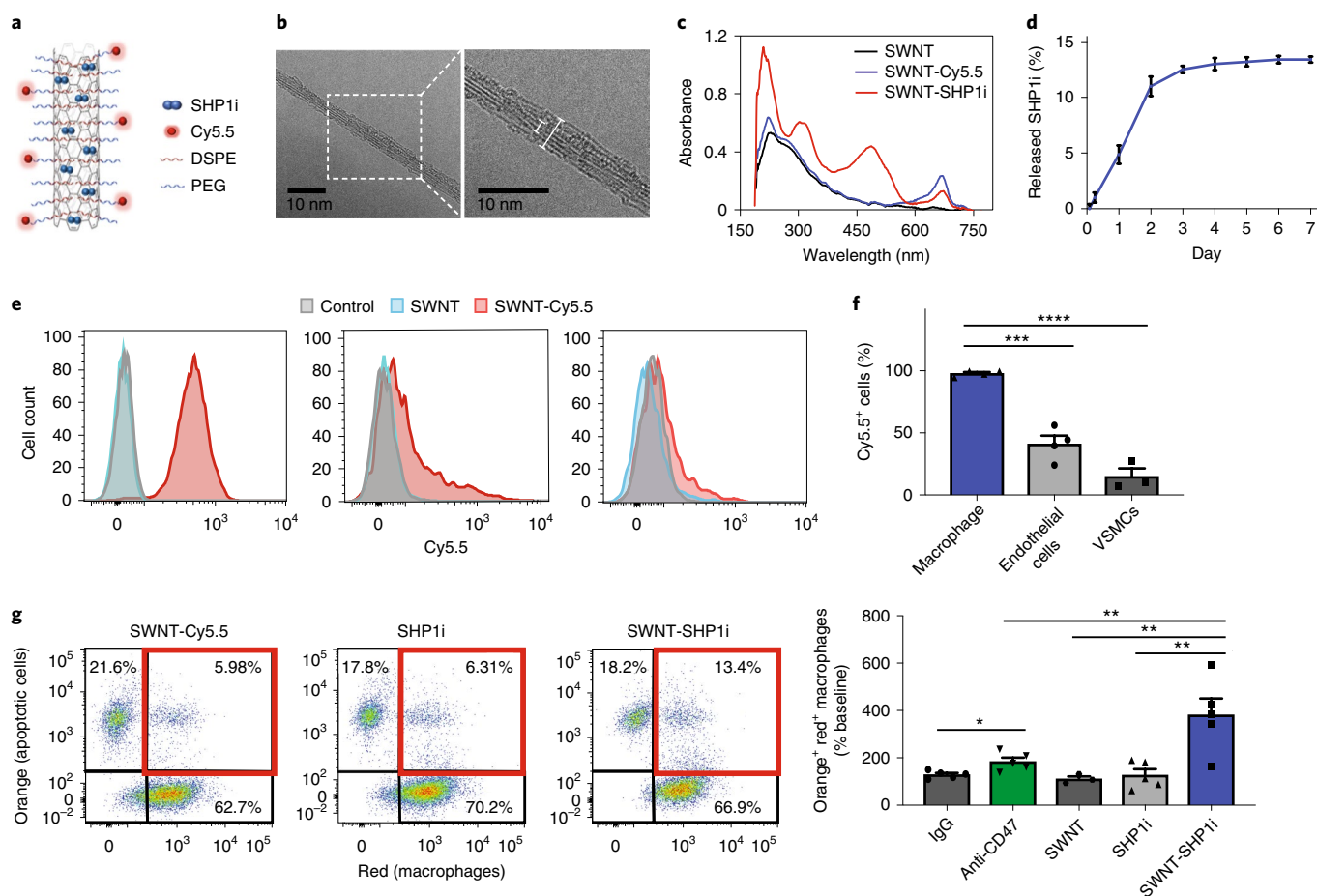


**Fig. 1 | SWNT-SHP1i promotes the phagocytosis of ACs by macrophages.** **a**, Schematic of SWNT-SHP1i, which comprises a backbone of SWNTs functionalized with phospholipid PEG (DSPE-PEG, 1,2-distearoyl-*sn*-glycero-3-phosphoethanolamine-*N*-[amino(polyethylene glycol)]) to form biocompatible nanotubes, Cy5.5 fluorophore for tracking in vivo delivery and SHP1i via  $\pi$ - $\pi$  stacking and hydrophobic interactions with the nanotube surface. **b**, Negative staining TEM images show the cylindrical morphology of SWNTs with their surrounding PEG phospholipid layer. Bare SWNTs apparently have a diameter of ~2–3 nm (inner white line). The adsorbed phospholipid PEG chains result in an increased SWNT diameter to ~5–6 nm (outer white line). Inset: magnified TEM image. **c**, Ultraviolet–visible spectra of SWNTs, SWNT-Cy5.5 and SWNT-SHP1i. **d**, Release curve of SHP1i from SWNT-Cy5.5 in serum, which demonstrates the controlled release over 7 days ( $n=3$  biologically independent experiments). **e**, Flow cytometry histograms of uptake studies with murine macrophages (RAW264.7) (left), endothelial cells (centre), and VSMCs (right). **f**, Cellular uptake assays demonstrate the propensity of SWNTs to specifically accumulate in murine macrophages (RAW264.7) ( $n$  = a minimum of three biologically independent experiments).  $***P=0.0001$  and  $****P<0.0001$  by one-way analysis of variance (ANOVA) with a Tukey post hoc test. **g**, In vitro phagocytosis assays confirm that SWNT-SHP1i augments the clearance of apoptotic vascular cells by macrophages at least as potently as the gold standard anti-CD47 antibodies, compared with SHP1i and SWNT-Cy5.5 controls ( $n=5$  biologically independent experiments). On the left are representative flow cytometry plots.  $*P<0.05$  by an unpaired two-tailed  $t$ -test and  $**P<0.01$  by one-way ANOVA with a Tukey post hoc test. For all the graphs, the data are expressed as the mean and s.e.m. IgG, immunoglobulin.

the inflammatory response, macrophages have a homeostatic role as phagocytes that scavenge lipids and apoptotic debris<sup>20</sup>. As their phagocytic capacity becomes impaired in advanced atherosclerosis, strategies that restore the ‘appetite’ of macrophages have the potential to both combat plaque expansion and prevent the inflammation that results from postapoptotic necrosis. We hypothesized that leveraging SWNTs as a ‘Trojan horse’ would enable us to achieve a plaque-specific modulation of the CD47-SIRP $\alpha$ -SHP-1 axis, and thereby promote the clearance of diseased cells in the lesion and minimize toxicities elsewhere in the body.

### Preparation and characterization of SWNT-SHP1i

After fabricating SWNT-PEG-Cy5.5 (SWNT-Cy5.5) as previously described<sup>16</sup>, we loaded them with a SHP1 inhibitor (SHP1i) (Fig. 1a and Extended Data Fig. 1). PEG was used to disperse SWNTs in aqueous solutions, endow biocompatibility and prolong in vivo

circulation times<sup>16</sup>. As shown by transmission electron microscopy (TEM) with negative staining, PEG functionalization resulted in well-dispersed cylindrical NPs with a PEGylated diameter of 5–6 nm, which included a 2–3 nm core nanotube structure (Fig. 1b). We employed fluorescent Cy5.5 dye for the flow cytometric characterization and loaded SHP1i onto SWNTs through  $\pi$ - $\pi$  stacking and hydrophobic interactions<sup>13</sup>. Ultraviolet–visible spectroscopy validated the presence of Cy5.5 (sharp peak at 674 nm) and SHP1i loading (absorption peaks at 230, 320 and 490 nm over the characteristic SWNT absorption spectrum) (Fig. 1c). The presence of Cy5.5 and SHP1i on the SWNTs was further confirmed by (1) the visible colour change in the SWNT-SHP1i solution on SHP1i adsorption, (2) attenuated total reflectance infrared spectroscopy (Extended Data Fig. 1) and (3) the shift in the  $\zeta$ -potential of SWNT-Cy5.5 from  $-6.69 \pm 2.11$  to  $-7.19 \pm 2.53$  mV on SHP1i loading. No endotoxin was detectable in the synthesized SWNT-SHP1i ( $<0.01$  ng ml<sup>-1</sup>).

To mimic *in vivo* biological conditions and simulate *in vivo* release, we studied the release profile of SHP1i from SWNT-Cy5.5 in serum (Fig. 1d). Similar to the release profile in PBS (Extended Data Fig. 1), SWNT-Cy5.5 demonstrated a sustained release of SHP1i for 7 days (nearly linear until day two; diminishing rates through day seven). The ability of this system to gradually offload substantial amounts of drug over a week suggest it may be suitable for delivering a sustained payload *in vivo*.

### SWNTs are taken up by macrophages and enhance AC phagocytosis *in vitro*

Although we have demonstrated the exquisite selectivity of SWNTs for circulating Ly-6C<sup>hi</sup> monocytes, their uptake by macrophages and other vascular cells has not yet been determined. Therefore, the propensity of SWNTs to be taken up by phagocytic cells was first examined in murine (RAW264.7) and human (THP-1) macrophages and compared to other vascular cells, such as endothelial and vascular smooth muscle cells (VSMCs). Using Cy5.5 positivity as a surrogate for uptake, flow cytometry revealed that SWNTs were robustly and preferentially taken up by >95% of macrophages relative to non-phagocytic cells (Fig. 1e,f and Extended Data Fig. 2).

To confirm their ability to inhibit CD47-induced signalling, we next studied the physiological properties of SWNT-SHP1i. *In vitro* phagocytosis assays confirmed that SHP1i-conjugated SWNTs potently stimulated the clearance of diseased vascular cells exposed to the pro-atherosclerotic tumour necrosis factor- $\alpha$  (Fig. 1g and Extended Data Fig. 2). Interestingly, when compared to anti-CD47 antibodies, SWNT-SHP1i yielded the highest degree of apoptotic-cell clearance. Further, SWNT-SHP1i did not alter the cell viability, proliferation rates or apoptosis of macrophages (Extended Data Fig. 2). Together, these data indicate that SWNTs stably facilitate the delivery of pro-efferocytic SHP1i specifically to macrophages, enhance their ability to clear ACs and do so without altering the cell physiology in other ways.

### SWNTs accumulate in atherosclerotic lesions *in vivo*

As we desire an agent that is not only taken up by phagocytes, but also delivers the pro-efferocytic payload to the atherosclerotic lesion, the biodistribution properties of SWNTs were next assessed. These studies were performed using a combination of radiochemical, flow cytometric and histological approaches in apolipoprotein-E-deficient (*apoE*<sup>-/-</sup>) mice with established plaques after a single systemic infusion of SWNTs labelled with Cy5.5 and/or <sup>89</sup>Zr. Pharmacokinetic analysis of <sup>89</sup>Zr-radiolabelled SWNTs demonstrated excellent serum stability and a blood half-life (*t*<sub>1/2</sub>) of 1.64 h (Fig. 2a and Extended Data Fig. 3). Consistent with prior reports that demonstrated SWNT distribution to organs of the reticuloendothelial system<sup>15,21,22</sup>, we observed a high initial uptake of radiolabelled SWNTs in macrophage-rich clearance organs, such as the spleen and liver 7 days postinjection (Fig. 2b). Flow cytometry analyses of the homogenized organs confirmed this distribution pattern, and demonstrated the specific accumulation of SWNTs locally within the microdissected plaque relative to the surrounding non-atherosclerotic aorta one week after treatment (Fig. 2c,d). Confocal microscopy further revealed significant SWNT accumulation within the atherosclerotic aortic sinus, with minimal to no accumulation in other non-clearance organs or the healthy aorta (Extended Data Fig. 3). No significant uptake was observed in the bone marrow, heart, lung, gut, fat, muscle and kidney (Fig. 2b,c).

### SWNTs are taken up by lesional macrophages

Prior studies in non-vascular mouse models revealed that >99% of the inflammatory Ly-6C<sup>hi</sup> monocytes (but <3% of other circulating immune cells) internalize SWNTs within two hours of administration<sup>16,23</sup>. To identify the specific vascular cell type(s) in which SWNTs chronically accumulate *in vivo*, we next performed high-

dimensional nine-colour flow cytometry of digested atherosclerotic aortae after a course of serial SWNT injections. After four weekly SWNT injections, ~70% of the lesional Ly-6C<sup>hi</sup> monocytes and ~60% of the macrophages had taken up SWNTs (versus only ~15% of the neutrophils, ~5% of the endothelial cells and ~5% of the fibroblasts). Negligible amounts of SWNTs were detected in the lymphocytes and VSMCs (Fig. 2e and Extended Data Fig. 4). Confocal microscopy confirmed that SWNTs co-localize with lesional macrophages (Fig. 2f and Extended Data Fig. 4). Flow cytometry showed that a greater percentage of the Ly-6C<sup>hi</sup> monocytes had taken up SWNTs in the atherosclerotic aorta than the spleen after 4 weeks of therapy (Fig. 2g). There are two major mechanisms that probably explain this pattern of uptake and robust plaque accumulation. First, SWNTs are taken up by circulating monocytes and traffic to the site of vascular inflammation, as occurs during atherogenesis<sup>17</sup>. Second, SWNTs passively target lesional macrophages (for example, extravasation through disrupted plaque vessels). Altogether, these data indicate that SWNTs chronically accumulate in the desired plaque-resident phagocytes.

### Pro-efferocytic SWNTs prevent atherosclerosis

To assess the therapeutic effect of SWNT-SHP1i on atherosclerosis, we employed two independent murine models of vascular disease (Extended Data Fig. 5). These included an accelerated inflammation model (dyslipidaemic *apoE*<sup>-/-</sup> mice implanted with subcutaneous angiotensin II-infusing minipumps<sup>24</sup>) and a chronic atherosclerosis model (*apoE*<sup>-/-</sup> mice fed a high-fat 'Western' diet for 11 weeks). Compared to the control treatment (SWNT-Cy5.5), treatment with SWNT-SHP1i via weekly injections resulted in a significant anti-atherosclerotic effect in both models and both sexes (Fig. 3a and Extended Data Figs. 5 and 6). Analysis of intraplaque SHP-1 phosphorylation (activity) confirmed that SWNT-SHP1i interrupts the key effector of antiphagocytic signalling downstream of CD47-SIRP $\alpha$  (Fig. 3b)<sup>25</sup>. To explore efferocytosis *in vivo*, lesions were assessed for their phagocytic index, or the number of ACs that were either 'free' or associated with macrophages due to efferocytosis<sup>6,26</sup>. Consistent with findings from *in vitro* phagocytosis assays, the ratio of free versus macrophage-associated ACs was lower in lesions from SWNT-SHP1i animals, which indicates an enhanced efferocytic activity in the vascular bed (Fig. 3c). As expected, lesions from SWNT-SHP1i-treated mice also displayed smaller necrotic cores (Fig. 3d) and a reduced accumulation of apoptotic bodies (Fig. 3e). These therapeutic benefits occurred independently of any changes in traditional cardiovascular risk factors, which included blood pressure, lipid and glucose levels (Extended Data Fig. 5).

Efficient efferocytosis also acts to resolve inflammation and prevent the secondary necrosis of dead cells<sup>2,27</sup>. To assess whether SWNT-SHP1i prevented the inflammatory consequences of defective efferocytosis, we next performed *in vivo* <sup>18</sup>F-fluorodeoxyglucose positron emission tomography/computed tomography (<sup>18</sup>F-FDG PET/CT) imaging (Supplementary Video 1)<sup>28</sup>. Mice treated with SWNT-SHP1i displayed a reduced aortic uptake of <sup>18</sup>F-FDG after treatment compared to the controls (Fig. 3f), which indicates decreased arterial inflammation. As persistent inflammation is known to promote plaque vulnerability and the risk for acute cardiovascular events, the apparent ability of pro-efferocytic SWNTs to combat inflammation is particularly intriguing.

### Single-cell RNA sequencing reveals an anti-inflammatory signature of SWNT-exposed macrophages

To assess the impact of chronic efferocytosis stimulation on lesional macrophages, large-scale single-cell RNA sequencing (scRNA-seq) was performed on leukocytes from the aortae of SWNT-Cy5.5- and SWNT-SHP1i-treated mice. After fluorescence-activated cell sorting (FACS) for Cy5.5<sup>+</sup> versus Cy5.5<sup>-</sup> cells, single-cell transcriptional profiles were obtained using droplet-based sequencing (Fig. 4a and

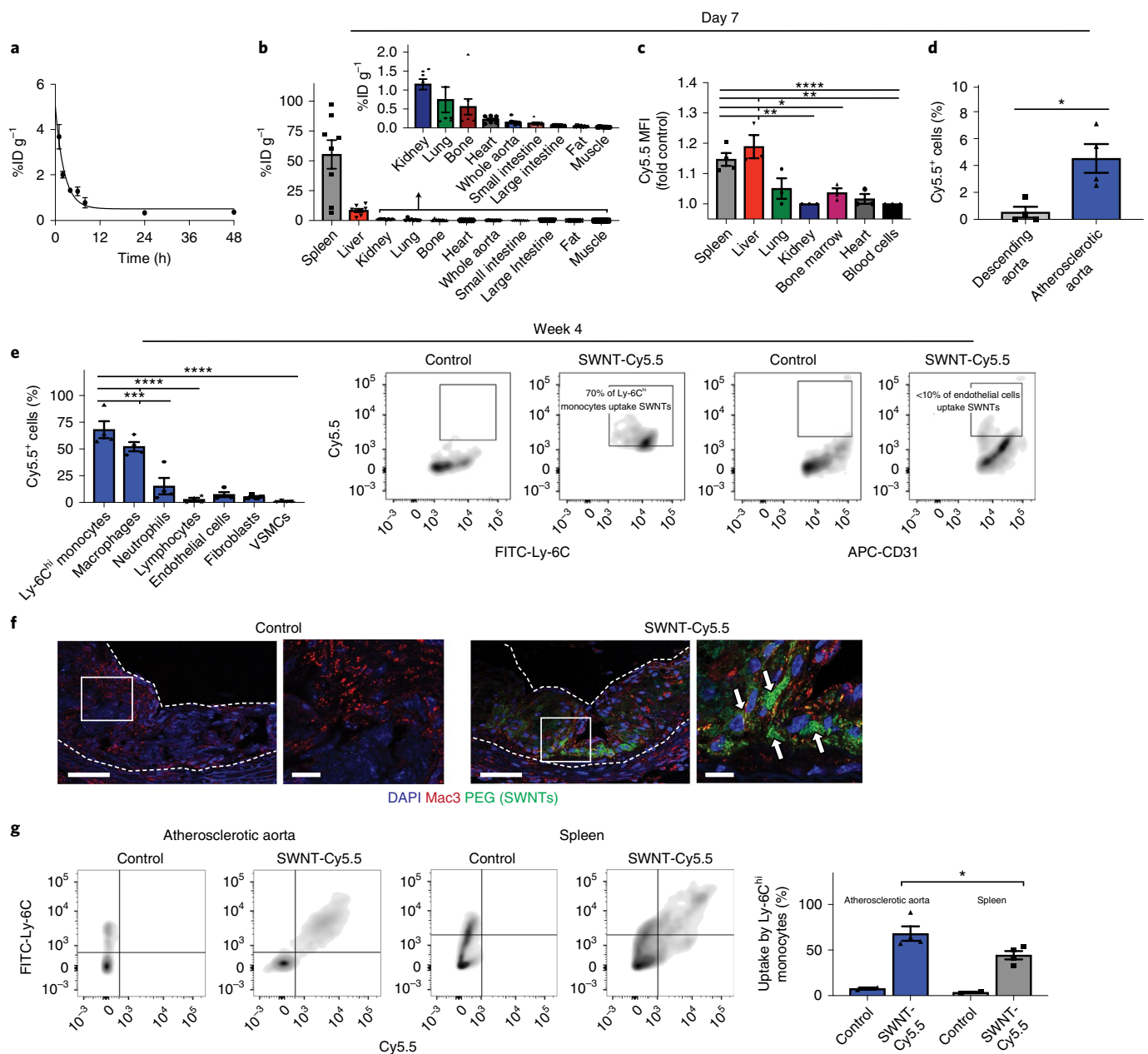


**Fig. 2 | SWNTs accumulate within phagocytes in the atherosclerotic plaque. a**, Blood decay curve of  $^{89}\text{Zr}$ -radiolabelled-SWNTs. The mean  $t_{1/2}$  was calculated as 1.64 h ( $R^2 = 0.96$ ,  $n =$  a minimum of four biologically independent animals per time point). %ID  $\text{g}^{-1}$ , percent injected dose per gram. **b**, Quantitative biodistribution studies 7 days after the intravenous administration of  $^{89}\text{Zr}$ -SWNTs reveal that SWNTs primarily accumulate in organs with a high macrophage content, such as the spleen and liver ( $n = 8$  biologically independent animals). **c, d**, Flow cytometry analyses of homogenized organs confirm the trend for an enhanced uptake by organs of the reticuloendothelial system (**c**), and reveal that SWNT accumulation is largely restricted to the macrophage-rich plaque, as compared to the less disease-prone descending aorta ( $n =$  minimum of three biologically independent animals) (**d**). \* $P < 0.05$ , \*\* $P < 0.01$ , \*\*\*\* $P < 0.0001$  by one-way ANOVA with a Tukey post-hoc test in **c**. \* $P < 0.05$  by an unpaired two-tailed  $t$ -test in **d**. **e–g**, Results after 4 weeks of weekly SWNT administration. **e**, SWNTs specifically accumulate within Ly-6C<sup>hi</sup> monocytes and macrophages in the atherosclerotic aorta, whereas SWNT detection is low in other vascular cells ( $n = 4$  biologically independent animals). \*\*\*\* $P < 0.0001$ , \*\*\*\* $P < 0.0001$  one-way ANOVA with a Tukey post hoc test. **f**, Lesional macrophage and SWNT co-localization was confirmed by confocal images of the aortic sinus (co-localized regions indicated by arrows). Scale bars, 50  $\mu\text{m}$ ; insets, 25  $\mu\text{m}$ . **g**, Enhanced uptake is observed by Ly-6C<sup>hi</sup> monocytes in the aorta compared to the spleen, which suggests that SWNTs may be efficiently delivered to the diseased artery by inflammatory monocytes ( $n = 4$  biologically independent animals). \* $P < 0.05$  by unpaired two-tailed  $t$ -test. The data in **f** are representative of four independent experiments. For all the graphs, the data are expressed as the mean and s.e.m. MFI, median fluorescence intensity.

Extended Data Fig. 7). After quality control and filtering, we analysed  $\sim 1,500$  immune cells with a mean of  $\sim 90,000$  sequencing reads per cell and expression quantified across 15,309 genes (Extended Data Fig. 7). Unsupervised clustering grouped cells according to

their expression pattern and detected seven distinct leukocyte clusters in the combined datasets from the aortae of SWNT-Cy5.5- and SWNT-SHP1i-treated mice (Fig. 4b,c). The major cell types were defined according to established immune cell markers and

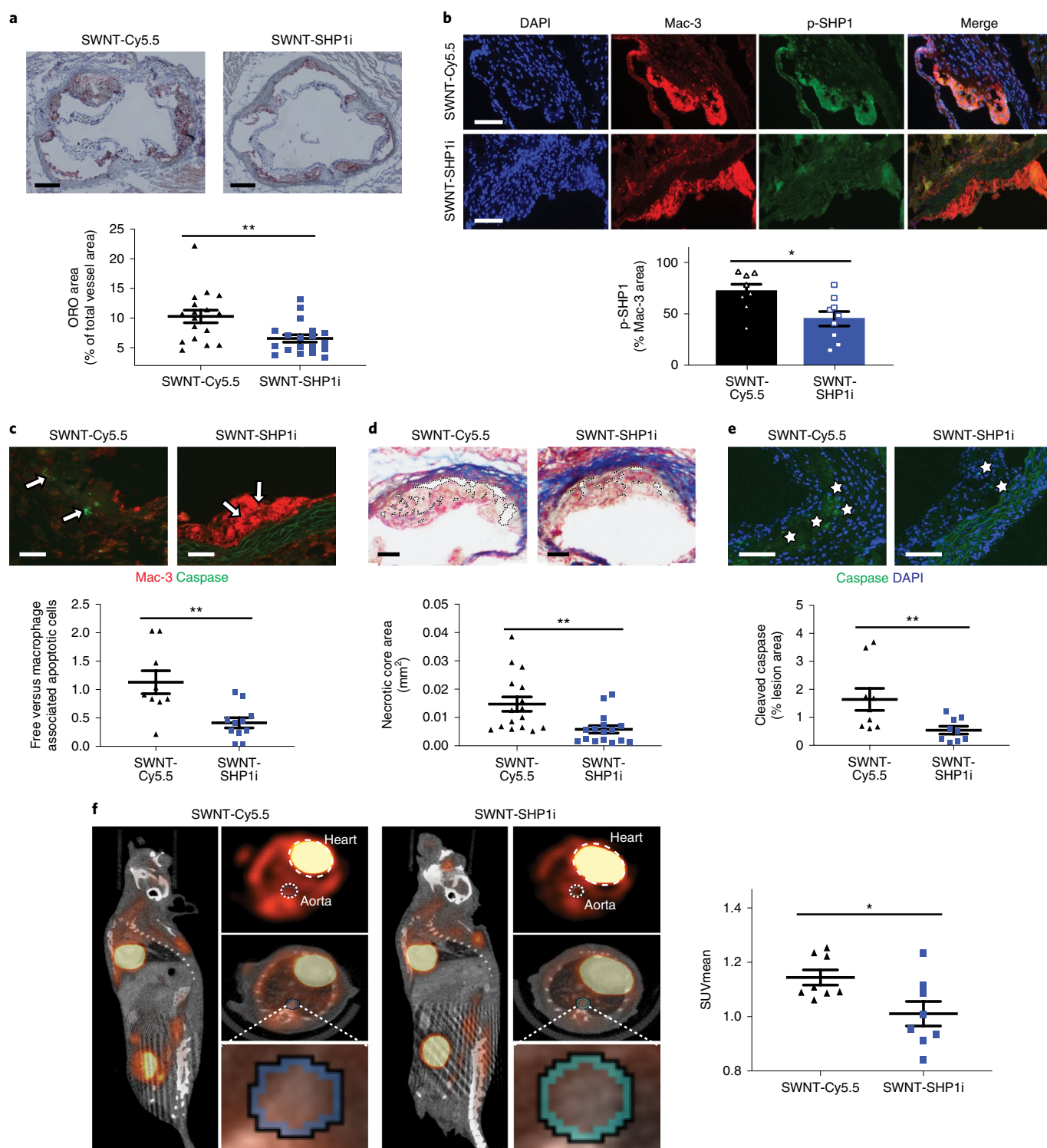


**Fig. 3 | Pro-efferoctytic SWNTs prevent atherosclerosis.** **a**, Mice treated with SWNT-SHP1i ( $n=19$ ) develop significantly reduced plaque content in the aortic sinus relative to SWNT-Cy5.5 controls ( $n=17$ ). These findings were confirmed in a second atherosclerosis model (Extended Data Fig. 5).  $**P < 0.01$  by a two-sided Mann-Whitney  $U$  test. Scale bar, 250  $\mu\text{m}$ . **b**, Compared to the control ( $n=8$ ), SWNT-SHP1i ( $n=9$ ) decreases the phosphorylation of SHP-1, which indicates silencing of the antiphagocytic CD47-SIRP $\alpha$  signal.  $*P < 0.05$  by an unpaired two-tailed  $t$ -test. Scale bars, 100  $\mu\text{m}$ . p-SHP1, phosphorylated SHP-1. **c–e**, Lesions from mice treated with pro-efferoctytic SWNTs are more likely to have ACs (indicated by arrows) that have been ingested by lesional macrophages ( $n=9$  biologically independent animals per group; scale bar, 25  $\mu\text{m}$ ) (**c**), develop smaller necrotic cores (indicated by dotted lines,  $n=16$  biologically independent animals per group; scale bar, 50  $\mu\text{m}$ ) (**d**) and accumulate less apoptotic debris (as assessed by the percentage of cleaved caspase-3<sup>+</sup> area in the plaque, indicated by stars,  $n=9$  biologically independent animals per group; scale bar, 50  $\mu\text{m}$ ) (**e**).  $**P < 0.01$  by an unpaired two-tailed  $t$ -test in **c** and by a two-sided Mann-Whitney  $U$  test in **d** and **e**. **f**, <sup>18</sup>F-FDG PET/CT imaging demonstrates that SWNT-SHP1i significantly reduces the vascular inflammation (Supplementary Video 1). For all graphs, the data are expressed as the mean and s.e.m. ORO, Oil Red O; DAPI, 4,6-diamidino-2-phenylindole; SUVmean, mean standardized uptake value.

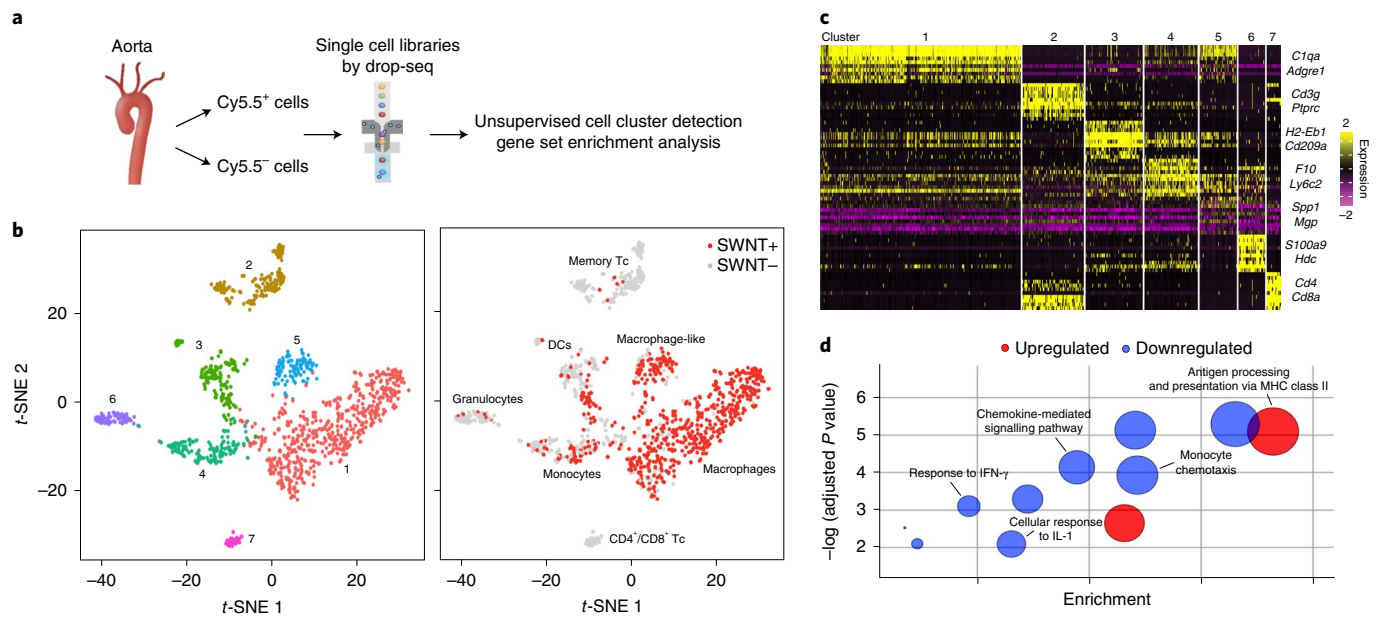


**Fig. 4 | Single-cell transcriptomics reveal genes and key molecular pathways modulated by a chronic CD47-SIRP $\alpha$  blockade in lesional macrophages.** **a**, Workflow for scRNA-seq which includes aortic cell isolation, drop sequencing and downstream analyses. **b**, Unsupervised dimensionality reduction identifies seven major cell types with a similar gene expression from the combined SWNT-Cy5.5 control and SWNT-SHP1i datasets ( $n = 4$  biologically independent animals per group). Data is visualized using  $t$ -distributed stochastic neighbour embedding ( $t$ -SNE) plots that show the seven distinct cell clusters (left) and SWNT detection in each cell (right). SWNT-positive cells are the most prevalent in lesional macrophages (Cluster 1) and macrophage-like cells (Cluster 5; Extended Data Fig. 7). Tc, T cells; DC, dendritic cells. **c**, Heat map showing the gene expression of ten cluster-defining genes and leukocyte markers (see Supplementary Table 1 for a full list of cluster markers). **d**, Single-cell differential gene expression analysis identifies the genes regulated by SWNT-SHP1i specifically in lesional macrophages ( $n = 4$  biologically independent animals per group). GO enrichment and pathway analyses reveal that the CD47-SIRP $\alpha$  blockade results in an increase in the expression of genes related to antigen processing and presentation, and the downregulation of genes associated with monocyte chemotaxis, chemokine signalling and the cellular response to the pro-inflammatory cytokines, IL-1 and interferon- $\gamma$  (IFN- $\gamma$ ). The subclasses of the top GO biological processes (fold enrichment  $>10$ , adjusted  $P$  value  $<10^{-2}$ ) are shown. The sizes of circles are proportional to the enrichment of each biological process. Functional enrichment was assessed using a two-sided Fisher's exact test with  $P$ -value adjustment by Bonferroni correction. MHC, major histocompatibility complex.

cluster-specific marker genes (Supplementary Table 1 and Extended Data Fig. 7), which identified macrophages (Cluster 1), memory T cells (Cluster 2), dendritic cells (Cluster 3), monocytes (Cluster 4), granulocytes (Cluster 6) and a mix of CD4<sup>+</sup>/CD8<sup>+</sup> cells (Cluster 7). Cluster 5 contained a 'macrophage-like' cell type that expressed myeloid-macrophage markers (*Cd68*, *Lgals3* and *Trem2*) and genes associated with SMCs and adventitial cells (*Spp1*, *Acta2* and *Mgp*)<sup>29</sup>.

After validation of the SWNT selectivity for macrophages by assessing the frequency of Cy5.5<sup>+</sup> cells in each cluster (Fig. 4b and Extended Data Fig. 7), differential expression analysis was performed to investigate the SWNT-SHP1i-dependent transcriptional response. Gene expression changes in FACS-sorted SWNT-positive cells were compared between treatment groups. We found that SWNT-SHP1i elicited numerous changes in lesional macrophages, which included a decrease in pro-inflammatory transcripts (*Ccl2*, *Ccl7*, *Ccl8* and *Pf4*) and an upregulation of genes linked to inflammation resolution (*Socs3* and *Zfp36*)<sup>30,31</sup> (Supplementary Table 2). Using the identified differential expression genes, we then applied a bioinformatics approach to explore the upstream regulators and functional significance of such alterations. As expected, both SIRPA ( $P = 3.26 \times 10^{-3}$ ) and the SHP-1 encoding gene, *PTPN6* ( $P = 4.05 \times 10^{-2}$ ) were predicted to mediate the observed transcriptional changes. Lesional SWNT-SHP1i-treated macrophages were enriched for genes associated with phagocytosis ( $P = 1.78 \times 10^{-7}$ ) and antigen presentation ( $P = 1.63 \times 10^{-7}$ ), a process known to be upregulated in macrophages engaged in necrotic cell clearance<sup>32</sup> (Supplementary Tables 3 and 4).

Pathway analyses also revealed that SWNT-SHP1i induced an expression signature in macrophages that reflects a decreased inflammatory response ( $P = 5.5 \times 10^{-13}$ ) and reduced chemotaxis of the mononuclear leukocytes ( $P = 2.6 \times 10^{-6}$ ). Interestingly, Gene Ontology (GO) enrichment analysis further showed that macrophages downregulated genes implicated in the response to interleukin-1 ( $P = 8.1 \times 10^{-3}$ ) and interferon- $\gamma$  ( $P = 7.85 \times 10^{-4}$ ) (Fig. 4d and Supplementary Tables 5 and 6). In accordance with our observations from PET/CT imaging, it appears that targeted efferocytosis stimulation may reduce vascular inflammation without resulting in serious complications, such as immunosuppression, as described below.

### Pro-efferocytic SWNTs have a favourable safety profile in vivo

Lastly, given that pro-efferocytic antibodies are compromised by adverse effects such as anaemia, the safety profile of SWNT-SHP1i was formally assessed. Previous studies showed that similarly PEG-functionalized SWNTs do not cause acute or chronic toxicities in mice, which encouraged further exploration of their applications in medicine<sup>14,15</sup>. SHP1i-conjugated SWNTs also appeared to be biocompatible and well-tolerated (Extended Data Fig. 8). Clinical haematology and chemistry results from SWNT-SHP1i-treated mice demonstrated no significant alterations, although there was a decrease in the platelet indices, platelet/large cell ratio and mean platelet volume (Extended Data Figs. 8 and 9). These indices are generally interpreted clinically in the context of thrombocytopenia or thrombocytosis<sup>33</sup>. Platelet levels of SWNT-SHP1i-treated

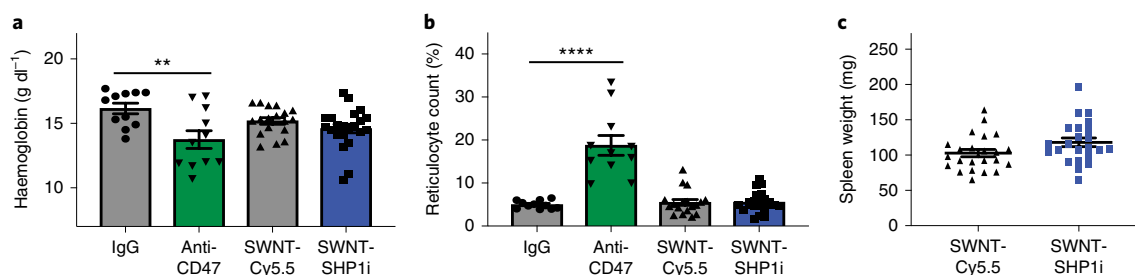


**Fig. 5 | Pro-efferoctytic SWNTs do not induce clearance of healthy tissue.** **a, b**, Mice treated with SWNT-SHP1i ( $n = 22$  biologically independent animals) do not develop anaemia (**a**) or a compensatory reticulocytosis (**b**), which occurs in response to anti-CD47-antibody treatment due to the off-target elimination of opsonized RBCs.  $**P < 0.01$ ,  $****P < 0.0001$  by an unpaired two-tailed *t*-test. **c**, No significant difference is observed for the weight of the spleen between groups, suggestive of the lack of RBC clearance due to Fc-dependent erythrophagocytosis ( $n = 23$  biologically independent animals per group,  $P = 0.065$ ). The IgG and anti-CD47 antibody data in **a** and **b** were reported previously ( $n = 11$  biologically independent animals per group)<sup>6</sup>. For all graphs, data are expressed as the mean and s.e.m.

animals, however, were in the normal range and there was no difference in bleeding or clotting events observed between treatment groups. SWNT-SHP1i treatment was also not associated with an increase in leukopenia, neutropenia or clinical infections. In addition, SWNT-SHP1i therapy was associated with a reduction in high-sensitivity C-reactive protein levels, a marker of inflammation and cardiovascular risk<sup>34</sup>.

Importantly, SWNT-SHP1i treatment was not associated with anaemia, the major complication that impedes the translation of pro-efferoctytic antibodies (Fig. 5a). Mice did not develop a compensatory reticulocytosis or splenomegaly (Fig. 5b,c), as occurs in response to an indiscriminate (systemic) CD47 blockade and the erythrophagocytosis of opsonized RBCs<sup>5,6,35</sup>. Of note, SHP-1 is primarily expressed in haematopoietic cells, where it negatively regulates multiple pathways in the immune response<sup>36</sup>. Global SHP-1 deficiency is known to cause defects in haematopoiesis and early mortality due to severe interstitial pneumonitis and glomerulonephritis<sup>37</sup>. Given that SWNT-SHP1i treatment did not demonstrate any of these potential toxicities (Extended Data Figs. 8 and 9), these data are consistent with the ability of SWNTs to avoid off-target effects due to their specific accumulation within monocytes and macrophages.

## Conclusions

Cardiovascular disease remains the world's leading killer. Most currently available therapies only target traditional risk factors (such as hypertension and hyperlipidaemia) and do not specifically inhibit the intrinsic, disease-causing pathways known to be active in the vessel wall. As the 'inflammatory hypothesis' of atherosclerosis is now definitively established<sup>34</sup>, and because robust genetic causation studies implicate defective efferocytosis as a key driver of plaque expansion<sup>38</sup>, new orthogonal therapies for these risk-factor-independent pathways are being sought. Although major progress has been made in developing agents that can suppress lesional inflammation (for example, anti-interleukin-1 $\beta$  (IL-1 $\beta$ ) antibodies) and/or the reactivate engulfment of apoptotic debris in the necrotic core (for example, anti-CD47 antibodies), each of these approaches has an Achilles heel that may limit its translational relevance. For example, the CANTOS trial revealed that systemic inhibition of the IL-1 $\beta$  pathway potentially reduced inflammation and recurrent major cardiovascular events (without altering the lipid levels), but unfortunately these benefits were offset by a concomitant increase in fatal infections<sup>34</sup>. Similarly, the first human trial of a pro-efferoctytic therapy recently provided tantalizing evidence that an anti-CD47 antibody might slow the progression of Hodgkin's lymphoma, but also came at a cost of increased anaemia, as expected<sup>35</sup>. Accordingly, a more precise targeting of these processes is required if

such cutting-edge therapies are to be broadly translated into the cardiovascular realm.

The advent of modifiable, macrophage-specific NPs therefore represents a significant advance in the fight against atherosclerosis. Although NPs have been developed for imaging and the treatment of atherosclerosis, the lack of sufficient selectivity of the NP to the target cell (for example, inflammatory monocytes) and desired end organ has hampered their efficacy and utility<sup>39,40</sup>. By combining innovations in vascular biology and nanotechnology, we engineered a Trojan horse system that accumulates in the lesional phagocyte, reactivates efferocytosis locally and reduces the plaque burden without inducing a significant off-target toxicity. SWNTs have also proved to be safe and non-immunogenic in non-human primates<sup>41</sup>, and mechanistic studies have revealed that SWNTs undergo elimination by immune cell peroxidases, such as myeloperoxidase, in a matter of weeks<sup>42,43</sup>. This biocompatibility is of crucial importance for the safety of SWNTs. Moreover, our scRNA-seq data indicate that pro-efferoctytic SWNTs have the unexpected benefit of suppressing cytokine-dependent vascular inflammation (without the undesirable immunosuppression associated with systemic anti-IL-1 $\beta$  therapy).

Although our current and previous studies<sup>16</sup> demonstrate the remarkable selectivity of SWNTs for monocytes and macrophages, further understanding of the mechanism of SWNT selectivity and incorporation of molecular targeting ligands may enable a more efficient delivery to the diseased site, or even to specific macrophage subsets. As the SWNT backbone can be modified to deliver multiple therapeutic agents into the same cell, future studies should determine whether bispecific nanoimmunotherapies that simultaneously target efferocytosis and other aspects of macrophage biology (for example, cholesterol efflux and macrophage skewing) might have a synergistic effect. In addition, unchecked inflammation in atherosclerosis results from the defective clearance of cells that have undergone multiple forms of cell death, such as necroptosis and pyroptosis<sup>44</sup>. Targeting the CD47-SHP1i pathway could thus restore the phagocytosis of apoptotic and non-AC debris that contribute to inflamed and unstable lesions. Future studies should address whether such pro-efferoctytic nanotherapies may promote plaque stabilization in advanced disease. Indeed, nanotherapeutics that promote local inflammation resolution have been shown to improve fibrous cap thickness and have a potent atheroprotective effect<sup>45</sup>. Given the parallels between plaque-resident and tumour-associated macrophages, it will be interesting to determine whether this platform could also be adapted as a precision therapeutic for the field of immuno-oncology.

## Online content

Any methods, additional references, Nature Research reporting summaries, source data, extended data, supplementary information,

acknowledgements, peer review information; details of author contributions and competing interests; and statements of data and code availability are available at <https://doi.org/10.1038/s41565-019-0619-3>.

Received: 1 March 2019; Accepted: 9 December 2019;

Published online: 27 January 2020

## References

- Arandjelovic, S. & Ravichandran, K. S. Phagocytosis of apoptotic cells in homeostasis. *Nat. Immunol.* **16**, 907–917 (2015).
- Huynh, M. L., Fadok, V. A. & Henson, P. M. Phosphatidylserine-dependent ingestion of apoptotic cells promotes TGF- $\beta$ 1 secretion and the resolution of inflammation. *J. Clin. Invest.* **109**, 41–50 (2002).
- Yurdagul, A. Jr., Doran, A. C., Cai, B., Fredman, G. & Tabas, I. A. Mechanisms and consequences of defective efferocytosis in atherosclerosis. *Front. Cardiovasc. Med.* **4**, 86 (2017).
- Jaiswal, S. et al. CD47 is upregulated on circulating hematopoietic stem cells and leukemia cells to avoid phagocytosis. *Cell* **138**, 271–285 (2009).
- Willingham, S. B. et al. The CD47-signal regulatory protein alpha (SIRP $\alpha$ ) interaction is a therapeutic target for human solid tumors. *Proc. Natl Acad. Sci. USA* **109**, 6662–6667 (2012).
- Kojima, Y. et al. CD47-blocking antibodies restore phagocytosis and prevent atherosclerosis. *Nature* **536**, 86–90 (2016).
- Leading Causes of Death, 1900–1998* (Centre for Disease Control and Prevention, 2015); [https://www.cdc.gov/nchs/data/dvs/lead1900\\_98.pdf](https://www.cdc.gov/nchs/data/dvs/lead1900_98.pdf)
- Heron, M. & Anderson, R. N. *Changes in the Leading Cause of Death: Recent Patterns in Heart Disease and Cancer Mortality* (National Center for Health Statistics, 2016); <https://www.cdc.gov/nchs/data/databriefs/db254.pdf>
- Brown, E. J. & Frazier, W. A. Integrin-associated protein (CD47) and its ligands. *Trends Cell Biol.* **11**, 130–135 (2001).
- Gresham, H. D. et al. Negative regulation of phagocytosis in murine macrophages by the Src kinase family member, Fgr. *J. Exp. Med.* **191**, 515–528 (2000).
- Liu, J. et al. Pre-clinical development of a humanized Anti-CD47 antibody with anti-cancer therapeutic potential. *PLoS ONE* **10**, e0137345 (2015).
- Weiskopf, K. et al. Engineered SIRP $\alpha$  variants as immunotherapeutic adjuvants to anticancer antibodies. *Science* **341**, 88–91 (2013).
- Liu, Z., Sun, X., Nakayama-Ratchford, N. & Dai, H. Supramolecular chemistry on water-soluble carbon nanotubes for drug loading and delivery. *ACS Nano* **1**, 50–56 (2007).
- Schipper, M. L. et al. A pilot toxicology study of single-walled carbon nanotubes in a small sample of mice. *Nat. Nanotechnol.* **3**, 216–221 (2008).
- Liu, Z. et al. Circulation and long-term fate of functionalized, biocompatible single-walled carbon nanotubes in mice probed by Raman spectroscopy. *Proc. Natl Acad. Sci. USA* **105**, 1410–1415 (2008).
- Smith, B. R. et al. Selective uptake of single-walled carbon nanotubes by circulating monocytes for enhanced tumour delivery. *Nat. Nanotechnol.* **9**, 481–487 (2014).
- Swirski, F. K. et al. Ly-6C<sup>hi</sup> monocytes dominate hypercholesterolemia-associated monocytosis and give rise to macrophages in atheromata. *J. Clin. Invest.* **117**, 195–205 (2007).
- Robbins, C. S. et al. Extramedullary hematopoiesis generates Ly-6C<sup>high</sup> monocytes that infiltrate atherosclerotic lesions. *Circulation* **125**, 364–374 (2012).
- Swirski, F. K. et al. Monocyte accumulation in mouse atherogenesis is progressive and proportional to extent of disease. *Proc. Natl Acad. Sci. USA* **103**, 10340–10345 (2006).
- Moore, K. J. & Tabas, I. Macrophages in the pathogenesis of atherosclerosis. *Cell* **145**, 341–355 (2011).
- Liu, Z. et al. In vivo biodistribution and highly efficient tumour targeting of carbon nanotubes in mice. *Nat. Nanotechnol.* **2**, 47–52 (2007).
- Campagnolo, L. et al. Biodistribution and toxicity of pegylated single wall carbon nanotubes in pregnant mice. *Part. Fibre Toxicol.* **10**, 21 (2013).
- Hung, S. C., Zhu, S., Ma, Z., Ghosen, E. & Mellins, E. D. Single-walled carbon nanotubes target neutrophils and Ly-6Chi monocytes and localize to joints in murine models of arthritis. *J. Immunol.* **175** (Suppl.), 23 (2018).
- Daugherty, A., Manning, M. W. & Cassis, L. A. Angiotensin II promotes atherosclerotic lesions and aneurysms in apolipoprotein E-deficient mice. *J. Clin. Invest.* **105**, 1605–1612 (2000).
- Zhang, Z., Shen, K., Lu, W. & Cole, P. A. The role of C-terminal tyrosine phosphorylation in the regulation of SHP-1 explored via expressed protein ligation. *J. Biol. Chem.* **278**, 4668–4674 (2003).
- Schrijvers, D. M., De Meyer, G. R., Kockx, M. M., Herman, A. G. & Martinet, W. Phagocytosis of apoptotic cells by macrophages is impaired in atherosclerosis. *Arterioscler. Thromb. Vasc. Biol.* **25**, 1256–1261 (2005).
- Poon, I. K., Lucas, C. D., Rossi, A. G. & Ravichandran, K. S. Apoptotic cell clearance: basic biology and therapeutic potential. *Nat. Rev. Immunol.* **14**, 166–180 (2014).
- Rudd, J. H. et al. Imaging atherosclerotic plaque inflammation by fluorodeoxyglucose with positron emission tomography: ready for prime time? *J. Am. Coll. Cardiol.* **55**, 2527–2535 (2010).
- Luo, G. et al. Spontaneous calcification of arteries and cartilage in mice lacking matrix GLA protein. *Nature* **386**, 78–81 (1997).
- Carballo, E., Gilkeson, G. S. & Blackshear, P. J. Bone marrow transplantation reproduces the tristetraprolin-deficiency syndrome in recombination activating gene-2 (–/–) mice. Evidence that monocyte/macrophage progenitors may be responsible for TNF $\alpha$  overproduction. *J. Clin. Invest.* **100**, 986–995 (1997).
- Yoshimura, A., Naka, T. & Kubo, M. SOCS proteins, cytokine signalling and immune regulation. *Nat. Rev. Immunol.* **7**, 454–465 (2007).
- Barker, R. N. et al. Antigen presentation by macrophages is enhanced by the uptake of necrotic, but not apoptotic, cells. *Clin. Exp. Immunol.* **127**, 220–225 (2002).
- George, T. I. *Automated Hematology Instrumentation* (UptoDate Inc., 2018).
- Ridker, P. M. et al. Antiinflammatory therapy with canakinumab for atherosclerotic disease. *N. Engl. J. Med.* **377**, 1119–1131 (2017).
- Advani, R. et al. CD47 blockade by Hu5F9-G4 and rituximab in non-Hodgkin's lymphoma. *N. Engl. J. Med.* **379**, 1711–1721 (2018).
- Plutzky, J., Neel, B. G. & Rosenberg, R. D. Isolation of a src homology 2-containing tyrosine phosphatase. *Proc. Natl Acad. Sci. USA* **89**, 1123–1127 (1992).
- Green, M. C. & Shultz, L. D. Motheaten, an immunodeficient mutant of the mouse. I. Genetics and pathology. *J. Hered.* **66**, 250–258 (1975).
- Kojima, Y. et al. Cyclin-dependent kinase inhibitor 2B regulates efferocytosis and atherosclerosis. *J. Clin. Invest.* **124**, 1083–1097 (2014).
- Smith, B. R. & Gambhir, S. S. Nanomaterials for in vivo imaging. *Chem. Rev.* **117**, 901–986 (2017).
- Flores, A. M. et al. Nanoparticle therapy for vascular diseases. *Arterioscler. Thromb. Vasc. Biol.* **39**, 635–646 (2019).
- Alidori, S. et al. Targeted fibrillar nanocarbon RNAi treatment of acute kidney injury. *Sci. Transl. Med.* **8**, 331ra339 (2016).
- Kagan, V. E. et al. Carbon nanotubes degraded by neutrophil myeloperoxidase induce less pulmonary inflammation. *Nat. Nanotechnol.* **5**, 354–359 (2010).
- Elgrabli, D. et al. Carbon nanotube degradation in macrophages: live nanoscale monitoring and understanding of biological pathway. *ACS Nano* **9**, 10113–10124 (2015).
- Green, D. R., Oguin, T. H. & Martinez, J. The clearance of dying cells: table for two. *Cell Death Differ.* **23**, 915–926 (2016).
- Fredman, G. et al. Targeted nanoparticles containing the proresolving peptide Ac2-26 protect against advanced atherosclerosis in hypercholesterolemic mice. *Sci. Transl. Med.* **7**, 275ra220 (2015).

**Publisher's note** Springer Nature remains neutral with regard to jurisdictional claims in published maps and institutional affiliations.

© The Author(s), under exclusive licence to Springer Nature Limited 2020

## Methods

**Preparation and characterization of SWNT-SHP1i.** The functionalized SWNTs were prepared as previously reported<sup>16</sup>, with slight modifications as follows. Raw HiPco (high-pressure catalytic decomposition of carbon) SWNTs (diameter 0.8–1.2 nm; Unidym) were added in an aqueous solution of DSPE-PEG<sub>5000</sub>-amine (NOF Corp), sonicated for at least 1 h and then centrifuged at 100,000g for 1 h to obtain PEGylated SWNTs. Unbound surfactant was washed by repeated filtration through 100 kDa filters (Millipore). For conjugation of Cy5.5 Mono NHS Ester (GE Healthcare) to SWNT-PEG, Cy5.5 Mono NHS Ester was incubated with SWNT-PEG solution (10:1 mole ratio) for 2 h. Excess Cy5.5 dye was removed by five to six rounds of centrifugal filtration until the filtrate became clear (Extended Data Fig. 1). SWNT concentrations were determined spectrophotometrically with an extinction coefficient of  $7.9 \times 10^6 \text{ M}^{-1} \text{ cm}^{-1}$  at 808 nm (refs 46,47). For SHP1i loading, the SHP1i solution was added to stirred SWNT-Cy5.5 at 4 °C and pH 7.4 overnight to form SWNT-SHP1i. After 24 h of stirring, SWNT-SHP1i was dialysed for another 24 h next to PBS to remove unbound SHP1i molecules. The concentration of the loaded SHP1i was measured using a NanoDrop (Nanodrop2000; Thermo Scientific) at its absorption of 320 nm.

To verify the synthesis of SWNT-SHP1i, after each step of the synthesis, ultraviolet-visible spectroscopy and attenuated total reflectance infrared spectroscopy in the 4,000–500  $\text{cm}^{-1}$  region (Nicolet iS50 FT/IR Spectrometer) were performed for PEGylated-SWNTs, SWNT-Cy5.5, SWNT-SHP1i and SHP1i. The surface charge of SWNT-Cy5.5 and SWNT-SHP1i were recorded in deionized water using a ZetaSizer Nano ZS (Malvern Instruments). Further SWNT characterization methods are given in the Supplementary Information.

**Preparation and characterization of <sup>89</sup>Zr-SWNTs.** Sulfo-SMCC solution (2 mg ml<sup>-1</sup>, 20  $\mu$ l) was added to 0.5 ml of SWNT-Cy5.5 (1  $\mu$ M) and stirred at room temperature for 2 h. Afterward, excess Sulfo-SMCC was removed by multiple washes using centrifugal filtration (100 kDa). A *p*-isothiocyanatobenzyl-deferoxamine (DFO) (2 mg ml<sup>-1</sup>, 200  $\mu$ l) solution in DMSO was then added to SWNT-Cy5.5-Sulfo-SMCC and incubated for 24 h. Extra chelators were washed by repeating the washing steps using centrifugal filtration (100 kDa). <sup>89</sup>Zr-oxalate (Stanford Cyclotron & Radiochemistry Facility) was diluted with PBS (pH 7.4) and a fraction of this solution was added to 0.5 ml of DFO-conjugated SWNT-Cy5.5 and incubated for 1 h at 37 °C with constant shaking. Excess <sup>89</sup>Zr was removed by centrifugal filtration (100 kDa) for 6–8 min at 4,000g. Instant thin-layer chromatography was used to determine the radiolabelling yield. A Capintec (CRC-15R) dose calibrator and Hidex gamma counter were used to measure the radioactivity of <sup>89</sup>Zr-SWNT-Cy5.5. The radiochemical purity was 100%. Serum stability experiments were performed at 37 °C in fresh mouse serum (Extended Data Fig. 3).

**TEM of SWNTs.** For SWNT-PEG negative staining, 10  $\mu$ l of 10 nM SWNT-PEG were drop cast onto ultrathin lacey carbon 400 mesh TEM grids (Ted Pella, Inc.) and incubated for 10 min. The grids were then washed with ultrapure water and negatively stained with 1% uranyl acetate for 30 s and subsequently dried on Whatman grade 1 filter paper. A Cs-corrected Titan TEM (Thermo Fisher Scientific) was operated with an acceleration voltage of 80 kV and a monochromator excitation value of 1. High-resolution TEM images were taken on a Gatan OneView camera via digital micrograph.

**Cell culture.** Mouse macrophages (RAW264.7, ATCC TIB-71) and mouse yolk sac endothelial cells (C166, ATCC CRL-2581) were grown in DMEM with 10% fetal bovine serum, whereas the human monocyte cell line (THP-1, ATCC TIB-202) was grown in RPMI-1640 medium that contained 10% fetal bovine serum and 0.05 mM 2-mercaptoethanol. Primary vascular SMCs were harvested from the aortae of C57Bl/6 mice and propagated in DMEM with 10% fetal bovine serum<sup>38</sup>. Human coronary artery SMCs (Lonza CC-2583) and human aortic endothelial cells (Lonza CC-2535) were cultured and maintained according to the manufacturer's (Lonza) instructions. All the cells were cultured in a humidified 5% CO<sub>2</sub> incubator at 37 °C. The cell lines were authenticated by the supplier. None of the cell lines were tested for mycoplasma contamination.

**SWNT in vitro uptake assay.** Cells were plated in 24-well plates (Corning) until approximately 70% confluent and then incubated with SWNT-Cy5.5 (4 nM) for 3 h in a serum-free media at 37 °C. SWNT-PEG and PBS-treated cells served as negative controls. After washing the cells with PBS, they were collected and analysed by flow cytometry (Scanford cell analyser, Stanford Shared FACS facility). Dead cells were excluded using SYTOX Blue stain (S34837; Invitrogen). The rate of SWNT uptake was evaluated by quantifying the percentage of Cy5.5<sup>+</sup> cells using FlowJo10.1.r5 (Tree Star, Inc.).

**Efferocytosis assay.** In vitro phagocytosis assays were performed as previously described<sup>6,38</sup>. Briefly, RAW264.7 macrophages were labelled with CellTracker Red (1  $\mu$ M; Life Technologies) and pretreated with SWNT (4 nM), SWNT-Cy5.5 (4 nM), SWNT-SHP1 (4 nM) or SHP1i (300 nM) for 30 min. For target cells, RAW264.7 cells or primary vascular SMCs were labelled with CellTracker Orange (1.25  $\mu$ M; Life Technologies) and incubated with tumour necrosis factor- $\alpha$  (50 ng ml<sup>-1</sup>; R&D

for 24 h to induce apoptosis. ACs were plated in 24-well dishes at a density of  $1.5 \times 10^5$  cells per well. RAW264.7 cells were added to cultured ACs at  $3 \times 10^5$  cells per well and co-incubated for 2 h in serum-free media. Anti-CD47 antibody (10  $\mu$ g ml<sup>-1</sup> MIAP410; BioXcell) was also tested as a positive control<sup>8</sup>. Cells were washed with PBS, dissociated from wells and analysed by flow cytometry (Scanford cell analyser). Efferocytic activity was evaluated as the percentage of phagocytes that were double-positive cells using FlowJo10.1.r5.

**Experimental animals.** *apoE*<sup>-/-</sup> mice on a C57Bl/6 background (Jackson Laboratory) were used in the following studies. A total of 136 male and female *apoE*<sup>-/-</sup> mice were included. All the animals were randomly assigned to the experimental groups. Animal studies were approved by the Stanford University Administrative Panel on Laboratory Animal Care (protocol 27279) and conformed to the National Institutes of Health (NIH) guidelines for the use of laboratory animals.

For the biodistribution studies, male *apoE*<sup>-/-</sup> mice were initiated on a high-fat Western diet (21% anhydrous milk fat, 19% casein and 0.15% cholesterol; Dyets Inc.) at 20–24 weeks of age and maintained on this for 4 weeks.

In the main atherosclerosis intervention studies, 8–10-week-old *apoE*<sup>-/-</sup> mice were implanted with subcutaneous osmotic minipumps (model 2004; Alzet) that contained angiotensin II (1,000 ng kg<sup>-1</sup> min<sup>-1</sup>; VWR) and initiated on a high-fat Western for the ensuing 4 weeks, as previously described (Extended Data Fig. 5)<sup>24</sup>. SWNT therapy began one day before osmotic pump implantation and continued weekly for the duration of the study. Both male and female animals were included as per recent NIH policy (Consideration of Sex as a Biological Variable, NOD-15-102). The 'angiotensin infusion' model was also used in the cellular specificity studies, <sup>18</sup>F-FDG PET/CT imaging and scRNA-seq.

In the chronic atherosclerosis studies, 8-week-old male *apoE*<sup>-/-</sup> mice were initiated on a high-fat diet and continued on this for the ensuing 11 weeks (without angiotensin II infusion). At 10 weeks of age, mice were injected as described above for a total of 9 weeks, and were euthanized at the age of 19 weeks.

**Flow cytometry of organs.** *apoE*<sup>-/-</sup> mice were injected a single dose of SWNT-SHP1i, SWNT-Cy5.5 or plain SWNTs (PEGylated but without Cy5.5) via the tail vein at a dose previously studied (200  $\mu$ l of 0.068 mg ml<sup>-1</sup> SWNTs)<sup>16</sup>. Mice were euthanized after 7 days, and the peripheral blood, bone marrow, aortae and visceral organs were collected. RBCs were removed from the peripheral blood with ammonium-chloride-potassium lysis buffer (Life Technologies). The aortae and visceral organs were homogenized and digested with Liberase TM (2 U ml<sup>-1</sup>; Roche) and Elastase (2 U ml<sup>-1</sup>; Worthington) in Hank's balanced salt solution at 37 °C for 1 h. Digested tissue was passed through a 70  $\mu$ m strainer to obtain single cell suspensions in 1% BSA/PBS and stained with SYTOX Blue. Fluorescence was detected by flow cytometry (Scanford cell analyser) and analysed using FlowJo10.1.r5. Cell populations were first gated for non-debris (forward scatter versus side scatter), then gated for singlets (forward scatter versus forward scatter width) and viable cells (SYTOX Blue<sup>negative</sup>) (Extended Data Fig. 3). The viable, single cells were analysed for Cy5.5 median fluorescence intensity, as well as Cy5.5 positivity to determine the percentage of Cy5.5<sup>+</sup> cells in each sample. The Cy5.5 median fluorescence intensity was normalized to the autofluorescence of each tissue type, as determined using samples from plain SWNT-injected mice.

**Pharmacokinetics and biodistribution studies.** The biodistribution studies were carried out at the treatment dose described above with 5–6 MBq of <sup>89</sup>Zr-labelled SWNTs. *apoE*<sup>-/-</sup> animals were sacrificed 7 days postinjection ( $n = 8$ ). The organs were collected into a preweighed vial and wet weighed. The blood  $t_{1/2}$  was measured by drawing 10  $\mu$ l of blood from the retro-orbital plexus at prespecified time points (1 h, 2 h, 4 h, 6 h, 8 h, 24 h and 48 h;  $n = 4$ –5 per time point). Pharmacokinetic analyses were performed by a first-order exponential decay fitting. All blood  $t_{1/2}$  and biodistribution samples were analysed for <sup>89</sup>Zr activity using a gamma counter (Hidex Automatic Gamma Counter) and then background and decay corrected to the injection time, converted into megabecquerel using calibrated standards and the %ID g<sup>-1</sup> determined by normalization to the total activity injected. A SpectraMax iD3 (Molecular Devices) was used for the fluorescence-based blood  $t_{1/2}$  study (excitation/emission, 678 nm/718 nm).

**SWNT cellular uptake profile.** Single-cell suspensions from the aortae and spleen were obtained as described above and incubated with anti-CD16/32 (553142; BD Biosciences) and stained on ice for 30 min with the following antibodies: Alexa Fluor 594-anti-Vimentin (clone EPR3776, ab154207; Abcam), APC-anti-CD31 (clone 390, 17-0311-80; Invitrogen), FITC-anti-Ly-6C (clone AL-21, 553104; BD Biosciences), PE-Cy5-labelled anti-CD5 (clone 53-7.3, 100609; BioLegend), PE-Cy7-anti-Gr-1 (clone RB6-8C5, 25-5931-81; Invitrogen), APC-Cy7-anti-CD11b (clone M1/70, 101225; BioLegend) and Pacific Blue-anti-F4/80 (clone BM8, 123123; BioLegend). For intracellular staining, cells were fixed and permeabilized with buffers (BD Phosflow Fix Buffer I and Perm Buffer III) according to the manufacturer's instructions, then stained with Alexa Fluor 488-anti-alpha-smooth muscle actin (clone 1A4, 50-112-4644; eBioscience). Cell suspensions were subjected to flow cytometry (Becton Dickinson LSR II) and analysed using FlowJo10.1.r5. Macrophages were identified as CD11b<sup>+</sup>/Ly-6C<sup>low</sup>/F4/80<sup>+</sup> cells.

Ly-6C<sup>hi</sup> monocytes were identified as CD11b<sup>+</sup>/Ly-6C<sup>hi</sup>/F4/80<sup>low</sup> cells. Neutrophils were identified as CD11b<sup>+</sup>/Gr-1<sup>hi</sup> cells.

**Atherosclerosis intervention studies.** To evaluate the therapeutic effect of pro-endothelial SWNTs, *apoE*<sup>-/-</sup> mice were treated with either SWNT-Cy5.5 or SWNT-SHP1i. Mice were treated weekly for four weeks in the angiotensin infusion model and for nine weeks in the chronic atherosclerosis studies (see timeline in Extended Data Fig. 5). Body weights were evaluated before and after treatment. Animals were observed daily, and in the case of premature sudden death, necropsy was performed to determine the cause of death. Blood pressure was measured in conscious mice at baseline and on a weekly basis throughout the study period (Visitech Systems). After treatment, mice were killed after an overnight fast, with their aortae, peripheral blood and visceral organs collected. The weights of the spleen, heart and kidney were recorded, as well as those of any unusually sized organs. Complete blood count, metabolic panel, high-sensitivity C-reactive protein and lipid profile determinations were performed by the Animal Diagnostic Laboratory in the Stanford Veterinary Service Center.

**Tissue preparation and immunohistochemical analysis.** For the aortic root analysis, mice were perfused with PBS via a cardiac puncture in the left ventricle and then perfusion fixed with phosphate-buffered paraformaldehyde (4%). Aortic roots and visceral organs were collected, embedded in OCT and sectioned at 7 µm thickness, starting from the base of the aortic root and covering the entire aortic sinus area. Four tissue sections at 100 µm intervals were collected from each mouse and stained with ORO (O1516; Sigma Aldrich). The lesion area was quantified from the luminal aspect of the blood vessel through the plaque to the internal elastic lamina (for example, lipid in the neointima was quantified) and was normalized to the total vessel area by encircling the external elastic lamina of the aortic wall. Necrotic core size and lesional collagen content were assessed with Masson's trichrome (Sigma Aldrich). The necrotic core was quantified by measuring the total acellular area within each plaque. Immunohistochemical staining for alpha-smooth muscle actin (ab5694, 1:300; Abcam) was performed for the analysis of the SMC content in the fibrous cap, with detection by the Vulcan Fast Red Chromogen kit (Biacare Medical). To assess the lesional SHP-1 activity, sections were co-stained with phospho-SHP1 (ab131500, 1:50; Abcam) and Mac-3 (BD 550292, 1:100; BD Sciences), followed by Alexa Fluor 488 and 594 (1:250; Life Technologies), respectively. The phospho-SHP1 area was quantified and normalized to the Mac-3 area<sup>6</sup>. To assess ACs in lesions, sections were stained for cleaved caspase-3 (Cell Signaling, 9661, 1:200) staining followed by Alexa Fluor 488 goat anti-rabbit (Life technologies, 1:250). The percentage of cleaved caspase-3<sup>+</sup> area was calculated and divided by the total atherosclerotic plaque area measured by ORO in serial sections. To study the phagocytosis of ACs by macrophages, the *in vivo* phagocytic index was calculated<sup>26</sup>. Sections were co-stained with cleaved caspase-3 and Mac-3, followed by Alexa Fluor. The phagocytic index was determined by manually counting the number of free ACs versus phagocytosed (macrophage-associated) ACs. For the detection of SWNTs, sections were stained with anti-PEG (PEG-B-47, ab51257, 1:100; Abcam). Frozen lung sections were stained with haematoxylin and eosin (H&E, Richard-Allan). C3 deposition in the kidney was assessed by staining sections with anti-mouse C3 (ab11862, 1:100; Abcam). Lesional SWNT co-localization images were taken on an inverted Zeiss LSM 880 laser scanning confocal microscope. All the other images were taken with a Nikon digital camera mounted on a fluorescent microscope and analysed using Adobe Photoshop CS6 in a blinded fashion.

**In vivo PET/CT imaging.** <sup>18</sup>F-FDG-PET/CT imaging was used to assess the changes in atherosclerotic inflammation in response to treatment with SWNT-SHP1i or control SWNT-Cy5.5 (*n* = 8 per group)<sup>28</sup>. The mice were fasted overnight prior to the scan. Special precautions were taken during the isoflurane-induced anaesthesia to maintain body temperature (before injection, after injection and during the scan). The radiotracer (15–20 MBq of <sup>18</sup>F-FDG; Stanford Cyclotron & Radiochemistry Facility) was administered intravenously to the mice. In addition, a long circulating formulation of iodinated triglyceride (Fenestra VC; MediLumine) was used as contrast agent. The mice were placed on the bed of a dedicated small animal positron emission tomography-computed Tomography (PET-CT) scanner (Inveon PET/CT; Siemens Medical Solution) 3 h after the <sup>18</sup>F-FDG administration, and a 30-min static PET scan was obtained. All the images were reconstructed using the OSEM algorithm. The same acquisition bed was used for the CT scan. The CT system was calibrated to acquire 360 projections (voltage 80 kV, current 500 µA). The voxel size was 0.206 × 0.206 × 0.206 mm<sup>3</sup>. Region-of-interest analysis was performed using IRW software (Inveon Research Workplace; Siemens). <sup>18</sup>F-FDG uptake in the thoracic aorta was quantified by drawing three-dimensional region-of-interests on the axial slices from the CT scan. The standardized uptake values were calculated and the mean value was used.

**Aortic single cell preparation for scRNA-seq.** Aortae (including the aortic sinus and aortic arch) were carefully dissected free from the perivascular adipose tissue and cardiac muscle, and then digested into single-cell suspensions as described above. Cells were pooled from mice treated with SWNT-SHP1i (*n* = 4) and SWNT-Cy5.5 (*n* = 4), and stained with SYTOX Blue to discriminate and exclude

non-viable cells. Viable cells (SYTOX Blue<sup>-</sup>) were sorted with a 100 µm nozzle into populations that were Cy5.5<sup>+</sup> and Cy5.5<sup>-</sup> using a BD Aria II and collected in PBS + 0.04% BSA.

**scRNA-seq and data analysis.** Samples were resuspended to a concentration of 600–1,000 cells µl<sup>-1</sup> in PBS + 0.04% BSA and loaded into the 10x Chromium system to generate single-cell barcoded droplets using the 10x Single Cell 3' reagent kit v2 (10x Genomics), according to the manufacturer's protocol. The resulting libraries were sequenced on an Illumina HiSeq4000 platform. Detailed methods on library preparation and sequencing are given in the Supplementary Information.

Single-cell RNA-sequencing data were preprocessed using 10x Cell Ranger software (Cell Ranger v3.0.2), which included data demultiplexing, barcode processing, alignment and single-cell 3' gene counting, as previously described<sup>48</sup>. Reads that were confidently mapped to the reference mouse genome (UCSC mm10) were used to generate a gene-barcode matrix for downstream analysis. The filtered gene-barcode matrices that contained only cell-associated barcodes were merged into a combined matrix from the above control (SWNT-Cy5.5) and treated (SWNT-SHP1i) datasets. Genes expressed in <5 cells, cells with <200 or >4,000 detected genes and cells with a percentage of mitochondrial genes >6% were filtered. After additionally filtering adventitial cells, 1,274 immune cells were included to assess the effect of chronic inhibition of the CD47-SIRPα-SHP1 axis. The resulting data was log-normalized, scaled and regressed on the number of unique molecular identifiers per cell and the percentage of mitochondrial gene content. Principle component analysis was performed for dimensionality reduction using the top 1,000 variable genes ranked by their dispersion from the combined datasets, followed by unbiased clustering analysis based on the identified PCs and *t*-SNE) for data visualization. To identify cell-type specific responses to the SWNT-SHP1i treatment, differential expression tests were performed for cell clusters to compare the samples from mice treated with SWNT-SHP1i and those with SWNT-Cy5.5. Differential expression genes with *P* < 0.05 based on the Wilcoxon rank sum test were considered statistically significant. All downstream analyses were performed with the Seurat R package v3.0 (ref. 49).

**Pathway analysis.** Pathway analysis was performed using significantly upregulated and downregulated genes between the SWNT-SHP1i and SWNT-Cy5.5 datasets. Genes were input for pathway analysis by Qiagen Ingenuity Pathway Analysis for the upstream regulator analysis and assessment of the enriched canonical pathways, diseases and functions, and PANTHER Pathway was used for the GO term enrichment analysis<sup>50</sup> (PANTHER overrepresentation test released on 13 November, GO ontology database released on 1 January 2019). GOPlot 1.0.2 was used for the visualization of results from the GO enrichment analysis.

**Statistical analysis.** Categorical data were compared using the Fisher's Exact Test. Continuous data are presented as mean ± s.e.m. and were tested for normality using the D'Agostino Pearson or Shapiro-Wilk test. Groups were compared using the two-tailed Student's *t*-test for parametric data and the Mann-Whitney U test for non-parametric data. When comparing more than two groups, data were analysed using ANOVA followed by Tukey post hoc tests. Measurements were taken from distinct samples. For atherosclerosis intervention studies, survival analysis was performed using the Kaplan-Meier method, with the log rank test used to compare time-to-mortality curves. A *P* value < 0.05 was considered to indicate statistical significance. Statistical analyses were performed using GraphPad Prism 7 (GraphPad Inc.).

**Reporting summary.** Further information on research design is available in the Nature Research Reporting Summary linked to this article.

## Data availability

The data that support the findings of this study are available from the corresponding author upon reasonable request.

## Code availability

Code used on R package for analysis of scRNA-seq data can be accessed by contacting A.M.F. at [aflores@stanford.edu](mailto:aflores@stanford.edu).

## References

- Liu, Z., Tabakman, S. M., Chen, Z. & Dai, H. Preparation of carbon nanotube bioconjugates for biomedical applications. *Nat. Protocols* **4**, 1372–1382 (2009).
- Smith, B. R. et al. Shape matters: intravital microscopy reveals surprising geometrical dependence for nanoparticles in tumor models of extravasation. *Nano Lett.* **12**, 3369–3377 (2012).
- Zheng, G. X. et al. Massively parallel digital transcriptional profiling of single cells. *Nat. Commun.* **8**, 14049 (2017).
- Butler, A., Hoffman, P., Smibert, P., Papalexi, E. & Satija, R. Integrating single-cell transcriptomic data across different conditions, technologies, and species. *Nat. Biotechnol.* **36**, 411–420 (2018).
- Ashburner, M. et al. Gene ontology: tool for the unification of biology. The gene ontology consortium. *Nat. Genet.* **25**, 25–29 (2000).

## Acknowledgements

A.M.F. is a Howard Hughes Medical Institute Research Fellow. K.-U.J. and P.T. are supported by Deutsche Forschungsgemeinschaft grant JA 2869/1-1:1 and TS 385/1-1. This study was funded by NIH R35 HL144475, R01 HL123370, a 2018 Fondation Leducq Award (to N.J.L.), K99 CA160764 (to B.R.S.), a Catalyst Award from the Dr. Ralph and Marian Falk Medical Research Trust, the Johnson Family Foundation (to N.J.L.) and the American Heart Association Transformational Project grant 18TPA34230113 (to B.R.S. and N.J.L.). We acknowledge the Stanford Small Animal Imaging Facility, the Stanford Cyclotron & Radiochemistry Facility, the Stanford Nano Shared Facilities/Stanford Nanofabrication Facility (National Science Foundation award ECCS-1542152) and the Stanford Shared FACS facility used for sorting (NIH S10 S10RR025518-01). The sequencing data were generated on an Illumina HiSeq 4000 that was purchased with funds from NIH S10OD018220. The authors acknowledge S. Gustafsson for help with bioinformatics analyses, I. Kalashnikova for technical assistance in nanocharacterization, T. Shaffer for radiochemistry assistance, D.-H. Chen for help with the TEM imaging, M. Weglarz of the Stanford FACS facility for technical support, D. Wagh of the Stanford Functional Genomics Facility for assistance with scRNA-seq and T. Doyle for valuable input on small animal imaging.

## Author contributions

B.R.S. and N.J.L. conceived the study. A.M.F. designed and conducted the majority of experiments. N.H.-N., K.-U.J., M.L. and B.R.S. developed, produced and characterized

SWNT-SHP1i. A.M.F., K.-U.J. and J.Y. performed the mouse microsurgery and histological analyses. A.M.F., N.H.-N., K.-U.J. and J.Y. conducted the flow cytometric and radiochemical biodistribution studies. K.-U.J. conducted the PET/CT imaging. X.Z. and B.R.S. performed the high-dimensional flow cytometry studies with assistance from A.M.F. and J.Y. N.H.-N., A.L.K., Y.Z., R.S. and B.R.S. performed and analysed the TEM. A.M.F. performed the scRNA-seq analysis with assistance from R.W. P.T., Y.W., V.N., Y.K., E.I. and I.L.W. contributed to experimental design and data interpretation. A.M.F., N.H.-N., K.-U.J., B.R.S. and N.J.L. wrote the manuscript. All the authors discussed the results and provided feedback on the manuscript.

## Competing interests

N.J.L. and I.L.W. are co-founders and hold equity interest in 47 Incorporated.

## Additional information

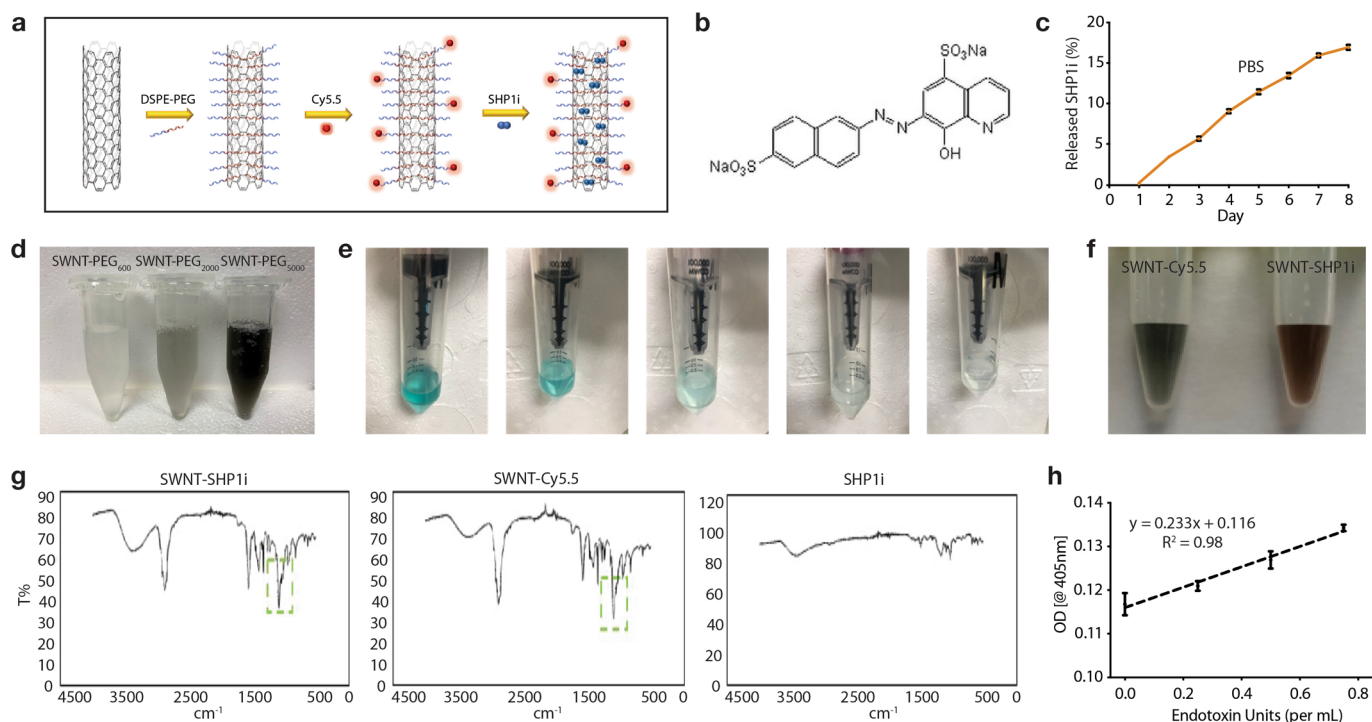
**Extended data** is available for this paper at <https://doi.org/10.1038/s41565-019-0619-3>.

**Supplementary information** is available for this paper at <https://doi.org/10.1038/s41565-019-0619-3>.

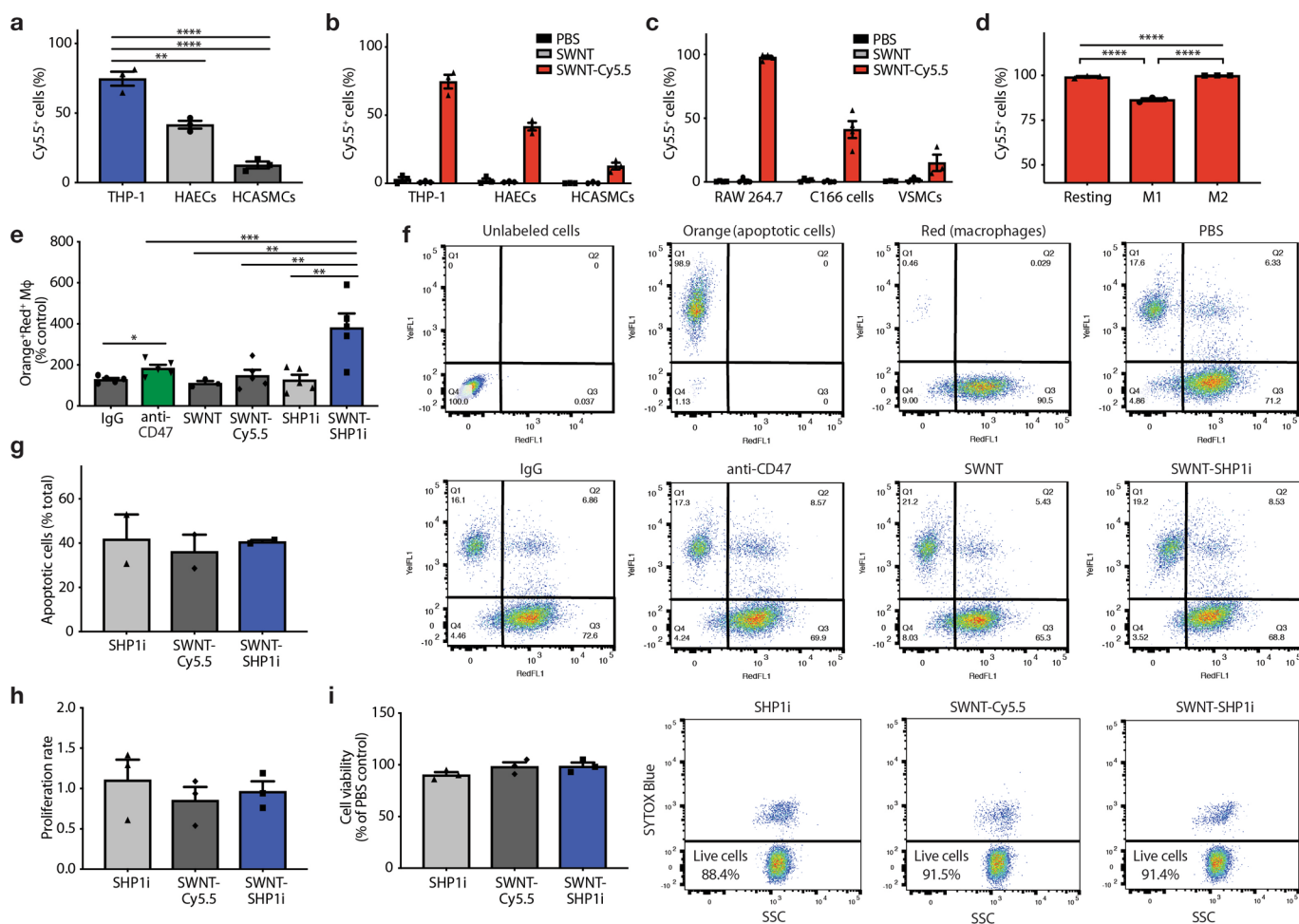
**Correspondence and requests for materials** should be addressed to B.R.S. or N.J.L.

**Peer review information** *Nature Nanotechnology* thanks Gabrielle Fredman, Willem Mulder and Edward Thorp for their contribution to the peer review of this work.

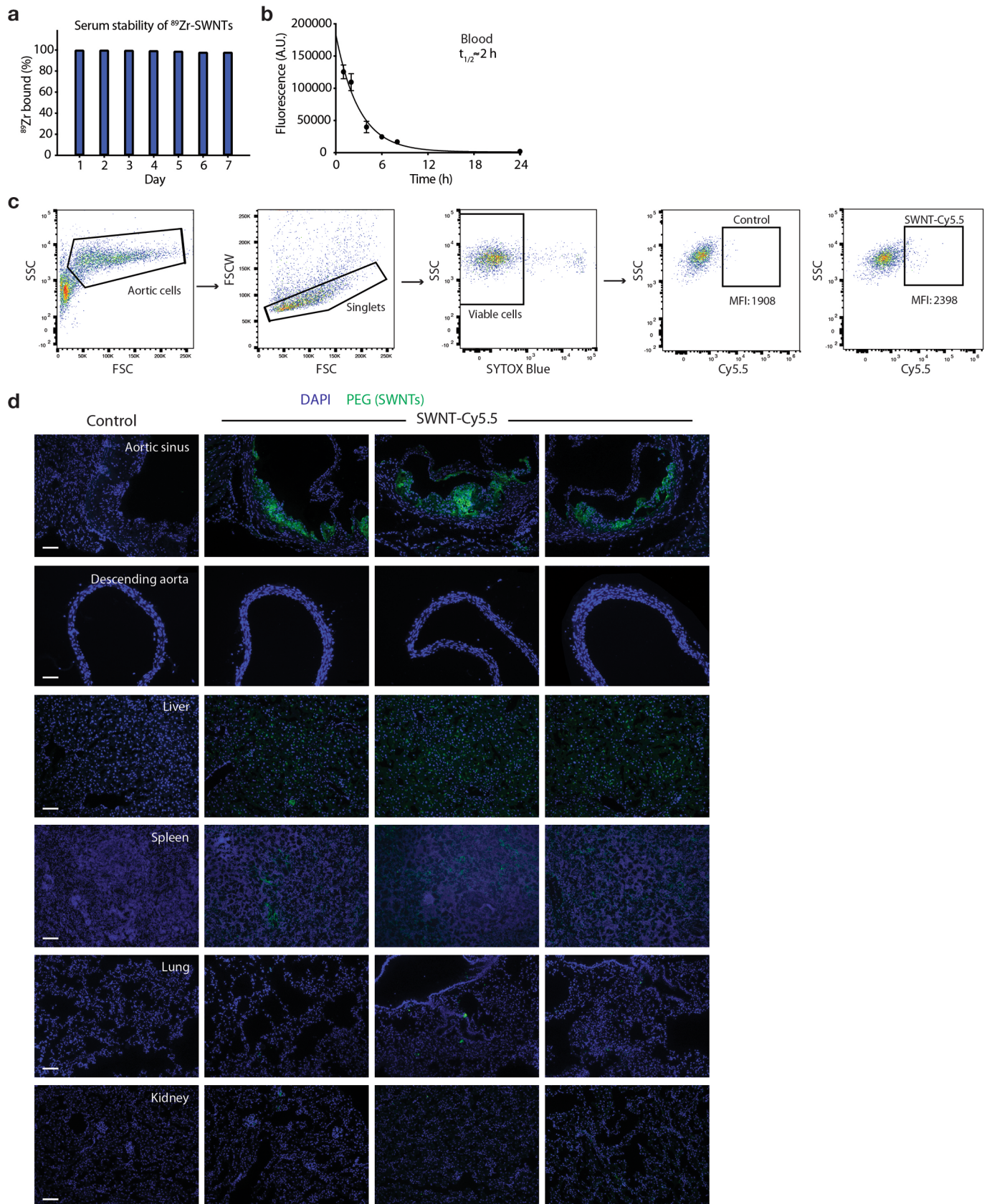
**Reprints and permissions information** is available at [www.nature.com/reprints](http://www.nature.com/reprints).



**Extended Data Fig. 1 | Extended Data Fig. 1. a**, Schematic illustrating steps of SWNT-SHP1i preparation. Following SWNT-PEG-Cy5.5 (SWNT-Cy5.5) fabrication, SHP1i is loaded onto SWNT-Cy5.5 by adding SHP1i to a stirred solution of SWNT-Cy5.5 overnight at 4 °C and removing free SHP1i molecules by dialyzing with PBS for 24h at 4 °C. DSPE-PEG: 1,2-distearoyl-sn-glycero-3-phosphoethanolamine-N-[amino(polyethylene glycol)]. **b**, Chemical structure of the small-molecule inhibitor of SHP-1. **c**, Release rates of SHP1i from SWNT-Cy5.5 in PBS (pH=7.4). **d**, Of the various PEG lengths tested, PEG<sub>5000</sub> provided the highest yield (3.5x higher than PEG<sub>2000</sub>). SWNTs were thus functionalized with PEG<sub>5000</sub> for in vitro and in vivo studies. **e-f**, Photos depicting color change in the SWNT-Cy5.5 filtrate demonstrating removal of excess Cy5.5 (blue color) after each washing step (**e**), and after loading SWNT-Cy5.5 with SHP1i (red-tinted solution on right) (**f**). **g**, Attenuated total reflectance (ATR) infrared spectra for SWNT-SHP1i, SWNT-Cy5.5, and SHP1i. The major spectral features of SHP1i are located in the fingerprint region, containing a complex set of absorptions. The S-O stretch from SO<sub>3</sub><sup>-</sup> in the SHP1i molecule observed at 1034 cm<sup>-1</sup> in SHP1i spectra is recapitulated in the SWNT-SHP1i spectrum as an additional spike at 1034cm<sup>-1</sup> in comparison with the SWNT-Cy5.5 spectrum (highlighted in square). These data confirm loading of SHP1i on SWNTs together with UV-vis spectra and the color change of the solution. Data in **c-g** were repeated 3 times with similar results. **h**, Quantification of endotoxin levels reveals that SWNT-PEG, SWNT-Cy5.5, and SWNT-SHP1i each have endotoxin levels <0.01 ng/mL (approximately 0.1 endotoxin units per mL; standard curve provided). The assay was performed once with 3 biological replicates. Mean and standard error of the mean (s.e.m.) are shown.

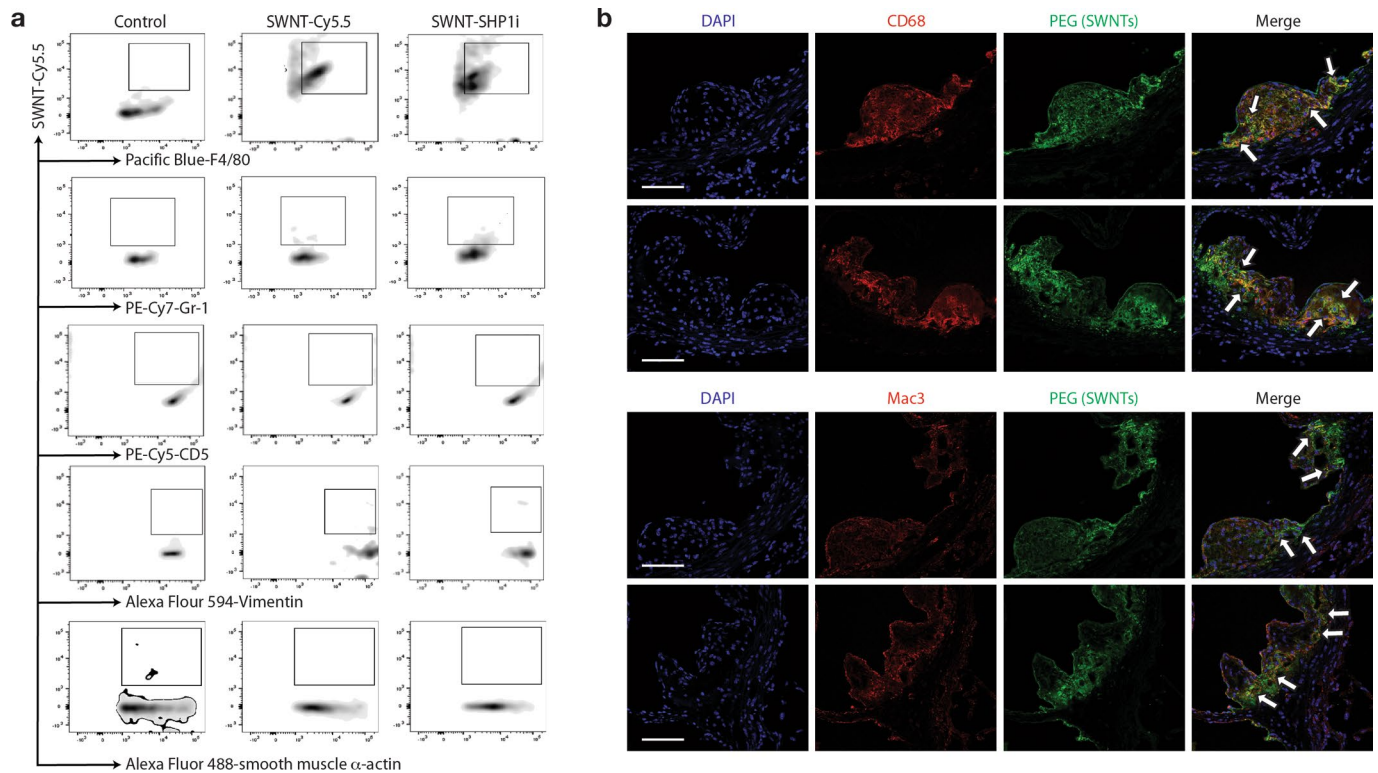


**Extended Data Fig. 2 | Extended Data Fig. 2. a-c**, In vitro uptake studies show that SWNTs are preferentially taken up by human and mouse macrophages after 3hr incubation. Uptake studies are shown in human macrophages (PMA-differentiated THP-1 cells), human aortic endothelial cells (HAECs), and human coronary artery smooth muscle cells (HCASMCs) (**a-b**,  $n = 3$ ), as well as murine macrophages (RAW264.7), endothelial cells (C166), and primary aortic vascular smooth muscle cells (VSMCs) (**c**,  $n =$  minimum 3 per cell type).  $**p < 0.01$ ,  $****p < 0.0001$  by one-way ANOVA with a Tukey post-hoc test. **d**, SWNTs are taken up by ~100% of basal (M0) and IL-4-polarized (M2) RAW264.7 macrophages, and ~85% of macrophages skewed towards the M1 state with LPS and IFN- $\gamma$  ( $n = 3$ ).  $****p < 0.0001$  by one-way ANOVA with a Tukey post-hoc test. **e**, The phagocytosis efficiency of macrophages (CellTracker Red<sup>+</sup>) against apoptotic vascular cells (CellTracker Orange<sup>+</sup>) is enhanced by SWNT-SHP1i nanoparticles, relative to SWNTs, SWNT-Cy5.5 and SHP1i controls ( $n = 5$ ).  $*p < 0.05$  by unpaired two-tailed t-test.  $**p < 0.01$ ,  $***p < 0.001$  by one-way ANOVA with a Tukey post-hoc test. **f**, Representative flow cytometry plots and staining controls for the conditions of the in vitro phagocytosis assays. Double-positive cells in the right upper quadrant represent macrophages that have ingested a target apoptotic cell. **g**, SWNT-SHP1i treatment does not alter the rates of programmed cell death of RAW264.7 macrophages in vitro, as shown by the lack of a difference in TUNEL (terminal deoxynucleotidyl transferase [TdT] dUTP nick-end labeling) staining ( $n = 2$ ). **h**, MTT assays show that SWNT-SHP1i has no effect on the proliferation rates of RAW264.7 macrophages in the presence of 10% serum ( $n = 3$ ). **i**, Cell viability assays indicate that SWNTs do not affect the viability of RAW264.7 cells, suggesting the absence of a toxic effect on macrophages ( $n = 3$ ). PBS served as control. Data in **f** are representative of 5 independent experiments. For all graphs, data are expressed as the mean and s.e.m.

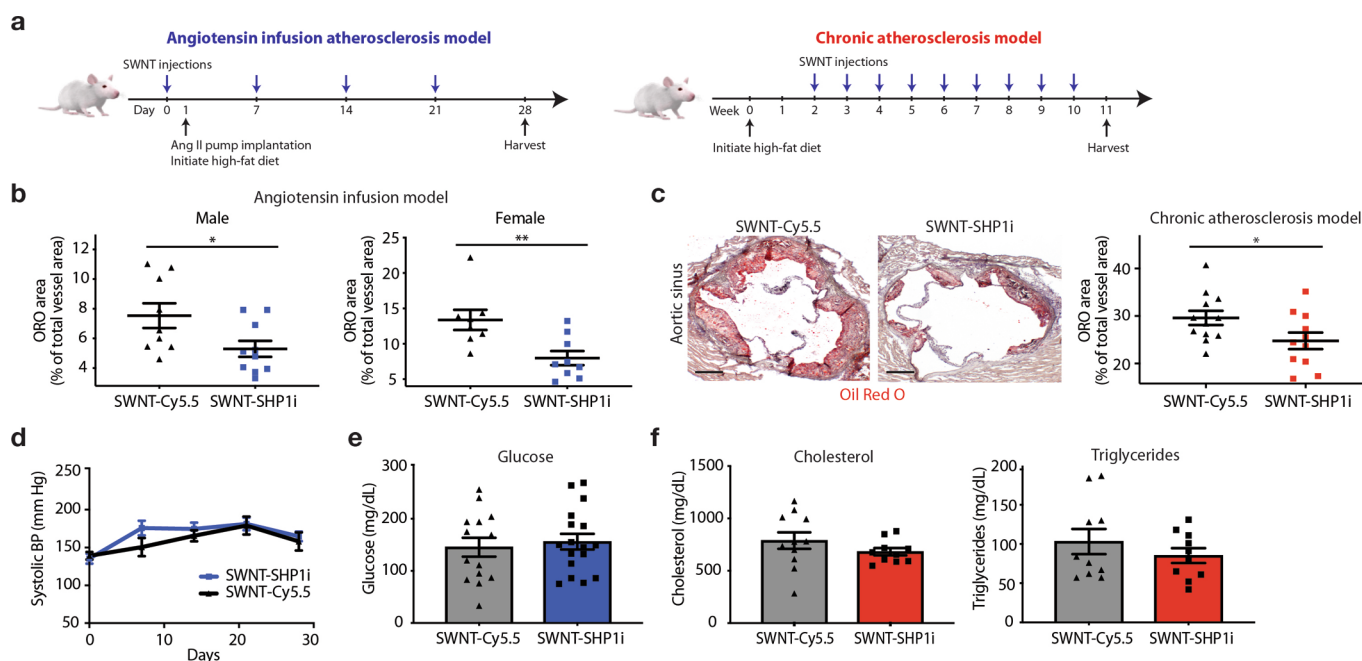


Extended Data Fig. 3 | See next page for caption.

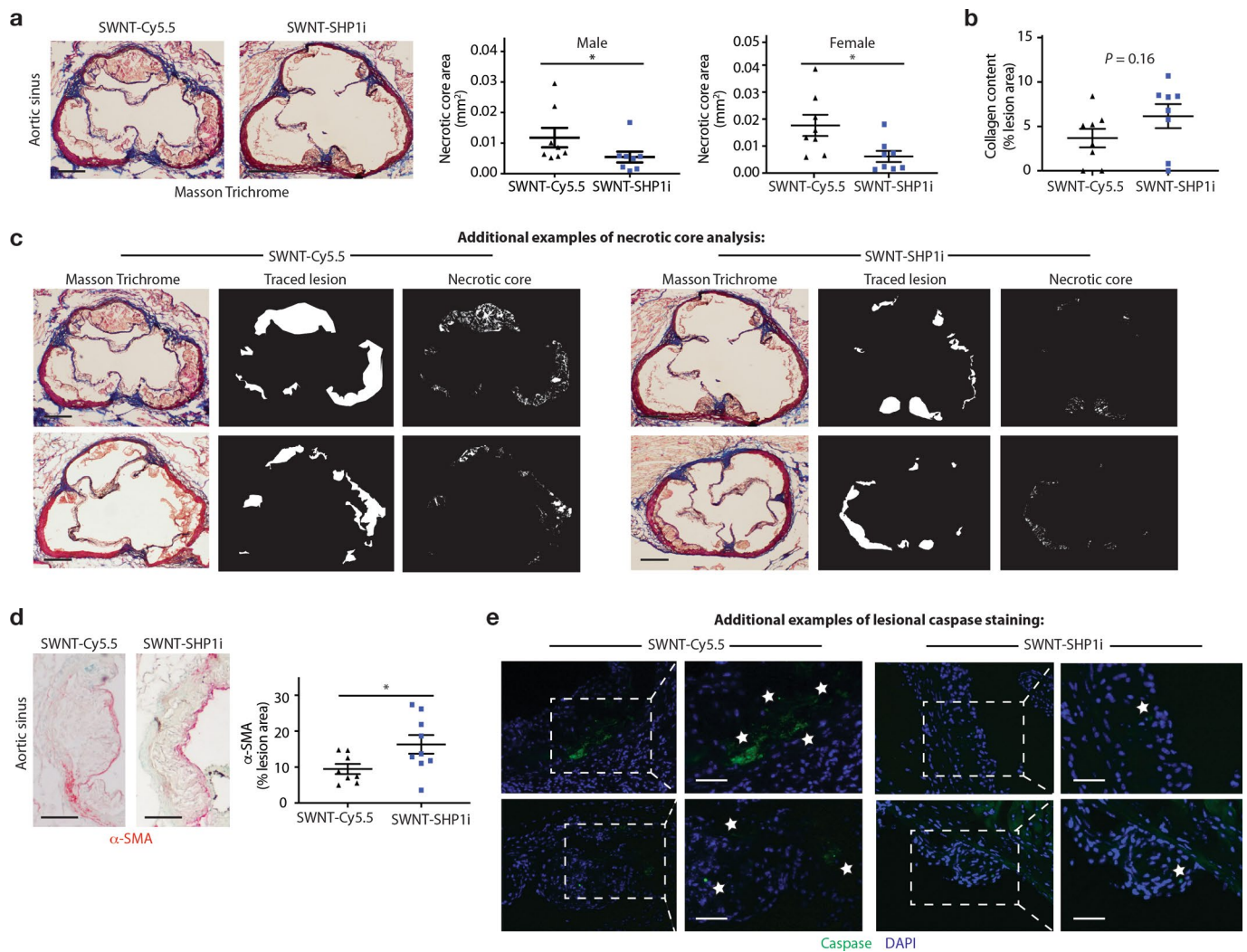
**Extended Data Fig. 3 | Extended Data Fig. 3. a**, Assessment of serum stability of  $^{89}\text{Zr}$ -radiolabeled SWNTs demonstrates no signs of instability for up to 7 days at 37°C in fresh mouse serum. Data are representative of 3 independent experiments. **b**, Fluorescence-based studies show that the blood half-life ( $t_{1/2}$ ) of SWNT-Cy5.5 measures ~2hr, indicating that desferrioxamine chelation of  $^{89}\text{Zr}$  to SWNT-Cy5.5 does not significantly alter the circulation time of the nanoparticles used in the formal biodistribution studies ( $n = \text{minimum } 4 \text{ biologically independent animals per time point}$ ). Mean and s.e.m. are shown. **c**, Representative flow cytometry plots and gating strategy for analysis of SWNT uptake in homogenized organs. **d**, Immunofluorescence imaging shows SWNT (immunostained for PEG) accumulation in the aortic sinus, with lesser amounts in the spleen and liver, and little-to-no accumulation in other organs such as healthy aorta, lung, and kidney after 4 weeks of weekly serial injections. Data are representative of a minimum of 3 independent experiments. Scale bars, 100  $\mu\text{m}$ .



**Extended Data Fig. 4 | Extended Data Fig. 4.** **a**, Representative flow cytometry plots from in vivo cellular uptake studies after 4 weeks of serial injections show significant SWNT accumulation in atherosclerotic Ly-6C<sup>hi</sup> monocytes and macrophages, but low uptake by other vascular cells ( $n = 4$  biologically independent animals). **b**, Additional confocal images demonstrate co-localization (indicated by arrows) of SWNTs (green) with macrophages (red) in the atherosclerotic aortic sinus. Macrophages were identified by immunostaining for both CD68 (top) and Mac-3 (bottom). Data are representative of 4 independent experiments. Scale bars, 50  $\mu\text{m}$ .

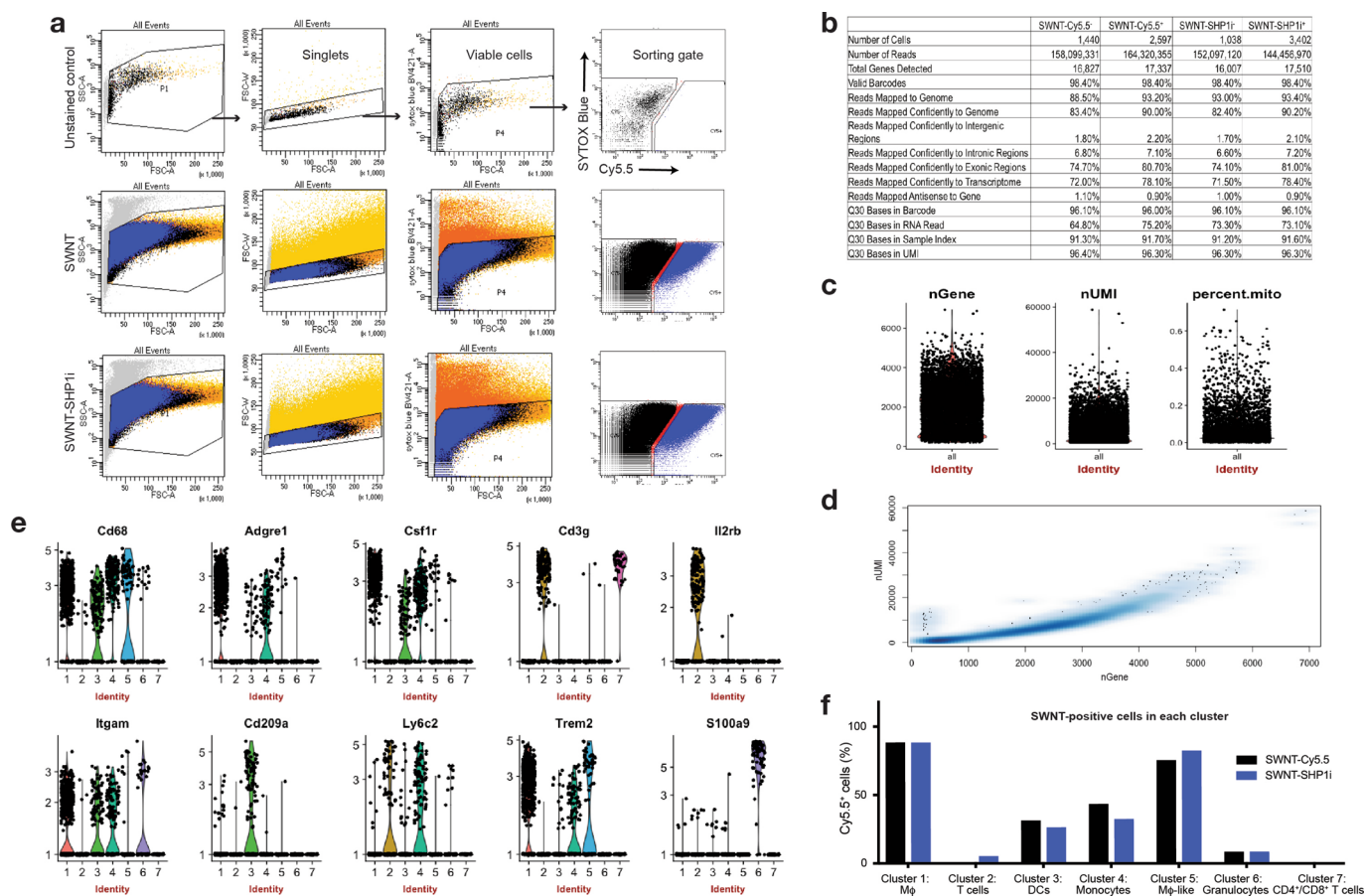


**Extended Data Fig. 5 | Extended Data Fig. 5. a**, Study timeline detailing the “angiotensin infusion” (which includes 4 weeks of high-fat diet and weekly SWNT injections) and “chronic atherosclerosis” models (which includes 2 weeks of high-fat diet, followed by 9 weeks of SWNT treatment without angiotensin II infusion). The beneficial effect of pro-efferocytic SWNT-SHP1i was confirmed in both models of vascular disease. **b**, In the main angiotensin infusion model, histological analysis of lesions in the aortic sinus area show that SWNT-SHP1i results in a significant reduction in plaque area in both male ( $n = 9$  biologically independent animals for control group,  $n = 10$  biologically independent animals for SWNT-SHP1i group) and female mice ( $n = 8$  biologically independent animals for control group,  $n = 9$  biologically independent animals for SWNT-SHP1i group), as measured by Oil Red O (ORO) staining. This finding is particularly important given the widely reported sex-dependent effects on atherosclerosis mouse models that is also relevant to human disease (Supplementary ref. 1).  $*p < 0.05$ ,  $**p < 0.01$  by unpaired two-tailed t-test. **c**, Similar therapeutic efficacy was observed in the chronic atherosclerosis models ( $n = 12$  biologically independent animals for control group,  $n = 11$  biologically independent animals for SWNT-SHP1i group).  $*p < 0.05$  by unpaired two-tailed t-test. Scale bar, 250  $\mu\text{m}$ . **d-f**, The benefits of pro-efferocytic SWNT-SHP1i on atherosclerosis occur independently of blood pressure ( $n = 6$  biologically independent animals per group) (**d**), glucose ( $n = 14$  biologically independent animals for control group,  $n = 17$  biologically independent animals for SWNT-SHP1i group) (**e**), and cholesterol levels ( $n = 11$  biologically independent animals for control group,  $n = 10$  biologically independent animals for SWNT-SHP1i group) (**f**). Blue graphs indicate results from the angiotensin infusion model, while red graphs indicated results from the chronic atherosclerosis studies. For all graphs, data are expressed as the mean and s.e.m.

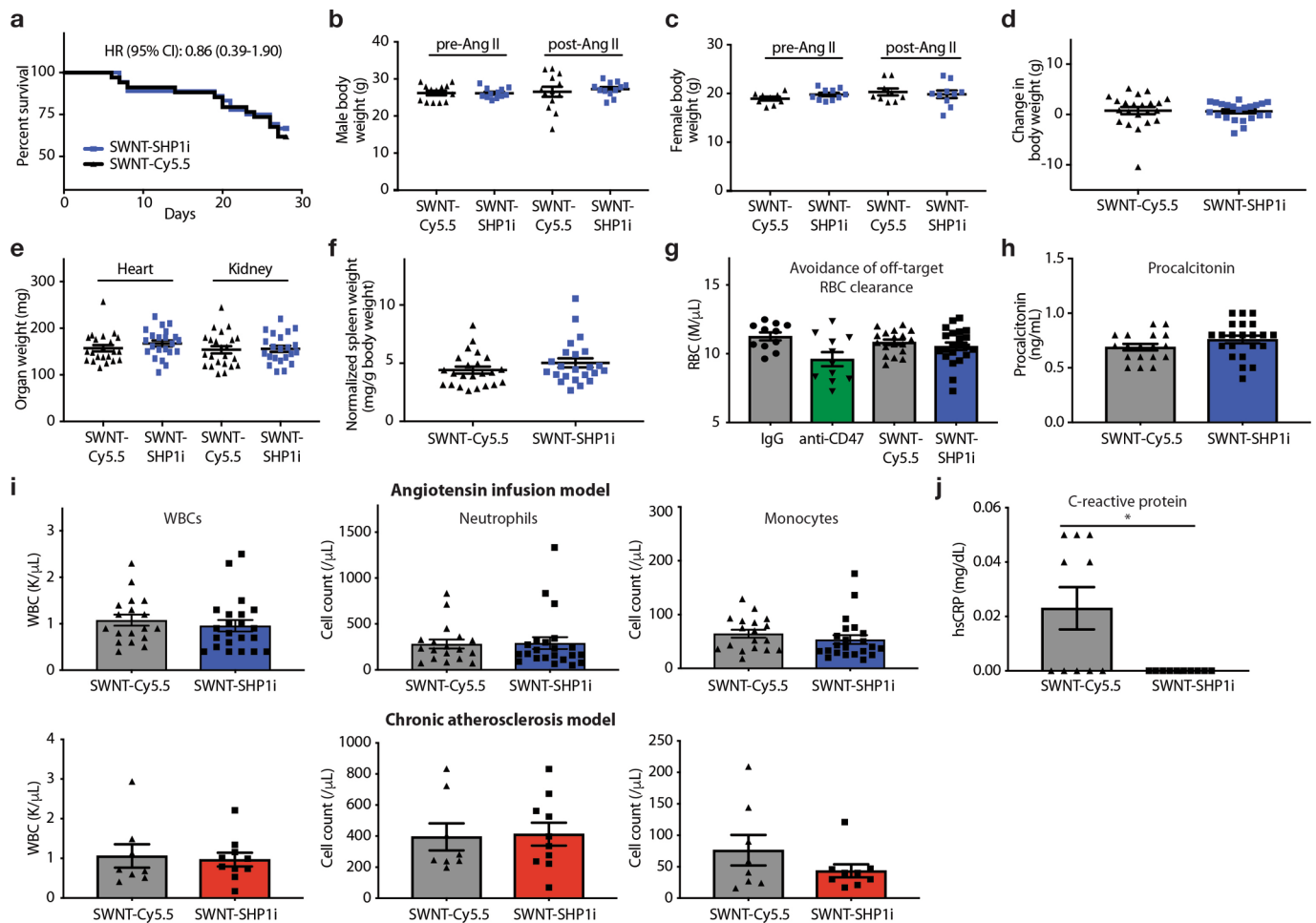


**Extended Data Fig. 6 | Extended Data Fig. 6.** Additional histological analyses confirm that SWNT-SHP1i induces a plaque-stabilizing phenotype.

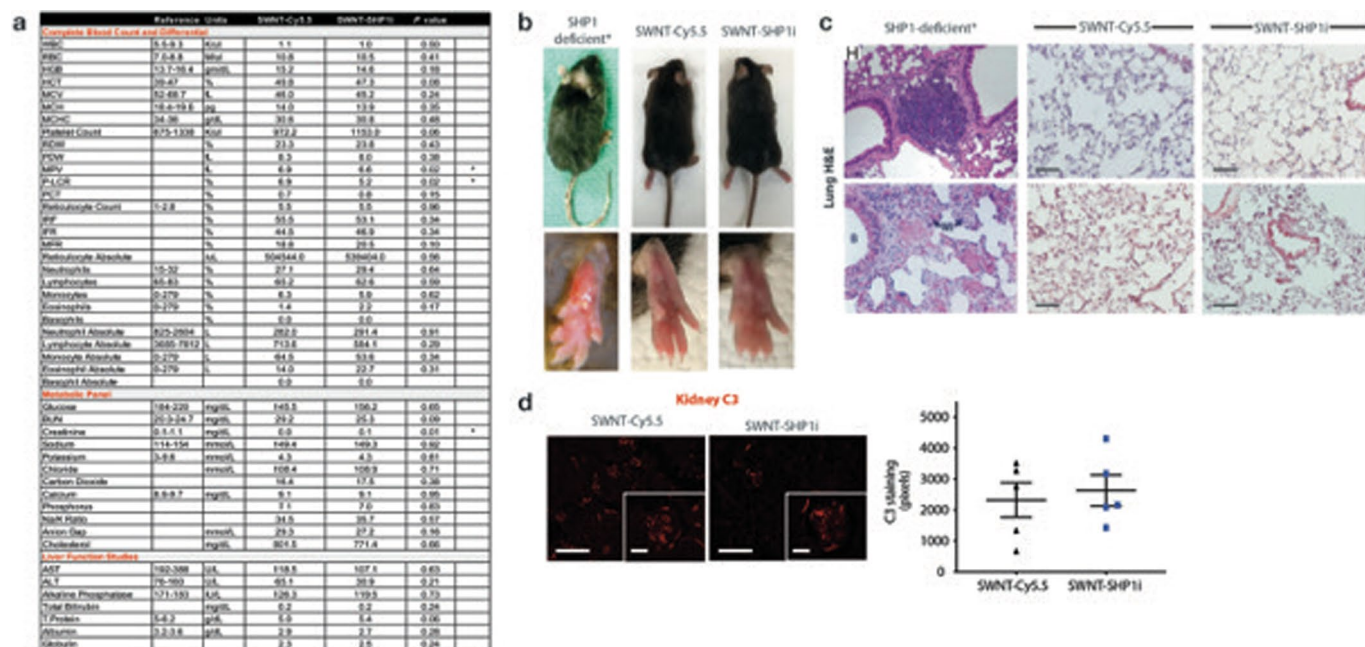
**a**, Masson Trichrome staining indicates that SWNT-SHP1i reduces the necrotic core in both male ( $n = 8$  biologically independent animals per group) and female mice ( $n = 8$  biologically independent animals per group).  $*p < 0.05$  by two-sided Mann-Whitney  $U$  test in left panel, by unpaired two-tailed  $t$ -test in right panel. Scale bar, 250  $\mu\text{m}$ . **b**, A trend towards increased collagen content was also observed after treatment ( $n = 8$  biologically independent animals per group). **c**, Additional examples of lesion tracing and necrotic core analyses indicating reduced accumulation of apoptotic and necrotic debris after treatment. Data are representative of 16 independent experiments. Scale bar, 250  $\mu\text{m}$ . **d**,  $\alpha$ -SMA staining indicates enhanced smooth muscle cell content in the cap, suggesting a reduction in plaque vulnerability after therapy ( $n = 8$  biologically independent animals for control group,  $n = 9$  biologically independent animals for SWNT-SHP1i group).  $*p < 0.05$  by unpaired two-tailed  $t$ -test. Scale bar, 250  $\mu\text{m}$ . **e**, Additional examples of lesional caspase staining (indicated with stars) highlighting a reduction in apoptotic cell content in treated animals. Data are representative of 9 independent experiments. Scale bar, 50  $\mu\text{m}$ . For all graphs, data are expressed as the mean and s.e.m.



**Extended Data Fig. 7 | Extended Data Fig. 7. a**, Flow cytometry gating strategy for selection of viable (SYTOX Blue-) cells that had taken up SWNTs (Cy5.5+). **b**, Sequencing data quality metrics for cells isolated from aortae of mice following treatment with SWNT-Cy5.5 or SWNT-SHP1i. **c**, Violin plots showing number of genes (nGene), unique molecular identifier (nUMI), and percentage of mitochondrial gene reads (percent.mito) for cells in the full dataset (n = 8 biologically independent animals). Each point represents the given value from a single cell. **d**, Scatterplot of nGene and nUMI across the combined dataset used to identify and exclude outliers (for example cell doublets). **e**, Representative violin plots showing the distribution of gene expression of immune cell markers in the 7 identified leukocyte clusters (n = 8 biologically independent animals). The identity of clusters was defined according to canonical hematopoietic-lineage and immune cell markers: macrophages (*Adgre1* encoding F4/80, *Cd68*, *Csf1r*), memory T cells (*Cd3g*, *Il2r*, *Ptprc* and *Il7r* encoding memory markers CD45RO and CD127), dendritic cells (*Cd209a*, *Flt3*, *Itgax* encoding CD11c), monocytes (*Ccr2*, *Ly6c2*, *Itgam* encoding CD11b), granulocytes (*Csf3r*, *S100a9*), and CD4<sup>+</sup>/CD8<sup>+</sup> T cell subsets (*Cd3e*, *Cd4*, *Cd8a*). Each point represents log-normalized single cell expression levels. **f**, Analysis of SWNT-positive (Cy5.5<sup>+</sup>) cells in each cluster confirms that SWNTs specifically target macrophages in the atherosclerotic aorta. Detection of SWNT uptake was greater in macrophages when characterizing cells by their whole-transcriptome, rather than the traditional limited markers used in flow cytometry above (Fig. 2e, Supplementary Fig. 4). ~90% of lesional macrophages took up SWNTs in both SWNT-Cy5.5 and SWNT-SHP1i treated animals as compared to <30% of dendritic cells and <10% of T cells and granulocytes with SWNT detection. Similarly high SWNT uptake (>75%) was detected in “macrophage-like” cells.



**Extended Data Fig. 8 | Extended Data Fig. 8.** **a**, Survival analysis indicate no change in mortality with SWNT-SHP1i treatment ( $n = 34$  biologically independent animals for control group,  $n = 36$  biologically independent animals for SWNT-SHP1i group). **b-d**, The in vivo safety of pro-efferocytic SWNTs is further supported by the stable body weight in *apoE*<sup>-/-</sup> mice treated with SWNT-SHP1i compared to SWNT-Cy5.5 controls ( $n = 22$  biologically independent animals per group). **e,f**, Similarly, there were no differences in the weight of any organ between groups ( $n = 22$  biologically independent animals per group). **g-j**, SWNT-SHP1i does not induce any major hematopoietic toxicities, such as the reduction in the red blood cell (RBC) count that is observed in anti-CD47 antibody treated mice (**g**). Procalcitonin levels are also unchanged between treatment groups, indicating a low likelihood for increased bacterial infections in SWNT-SHP1i-treated mice (**h**). There is also no effect of SWNT-SHP1i on total leukocytes, neutrophils, or monocytes ( $n = 18$  biologically independent animals for control group,  $n = 22$  biologically independent animals for SWNT-SHP1i group) (**i**). Lastly, without inducing immunosuppression, SWNT-SHP1i reduced hs-CRP levels, suggesting reduced inflammation after treatment ( $n = 10$  biologically independent animals per group). \* $p = 0.03$  by two-sided Mann-Whitney *U* test (**j**). Blue graphs indicate results from the angiotensin infusion model, while red graphs indicate results from the chronic atherosclerosis studies. Data from anti-CD47 and IgG-treated mice in (**g**) are previously reported ( $n = 11$  biologically independent animals per group), see Supplementary ref. 2. For all graphs, data are expressed as the mean and s.e.m.



**Extended Data Fig. 9 | Extended Data Fig. 9. a**, Hematology assessment demonstrate that SWNT-SHP1i treatment results in a significant decrease in the mean platelet volume (MPV) and platelet-large cell ratio (P-LCR), but has no effect on major parameters of the complete blood count or metabolic panel that would indicate organ or hematopoietic toxicity (n = minimum 9 biologically independent animals per group). \**p* < 0.05 by unpaired two-tailed t-test. **b-d**, In contrast to prior publications indicating that global knockout of SHP-1 can have a variety of harmful effects including dermatitis, pneumonitis, and renal complement deposition (images adapted from Supplementary refs. 3,4,5), we observed none of these toxicities in mice treated with macrophage-specific SWNT-SHP1i<sup>6</sup>. This favorable safety profile was evidenced by a lack of hair loss or suppurative skin lesions (**b**), an absence of pulmonary inflammation and alveolar hemorrhage (**c**), and the absence of elevated renal C3 immunofluorescence staining (n = 5 per group, 4 sections analyzed per animal) (**d**). Scale bar in **c**, 100µm. Scale bars in **d**, 200 µm and 50 µm (insets). SHP1-deficient image in **9c** reprinted with permission from Supplementary ref. 4; Copyright (2008) National Academy of Sciences, U.S.A. For all graphs, data are expressed as the mean and s.e.m.

## Reporting Summary

Nature Research wishes to improve the reproducibility of the work that we publish. This form provides structure for consistency and transparency in reporting. For further information on Nature Research policies, see [Authors & Referees](#) and the [Editorial Policy Checklist](#).

### Statistics

For all statistical analyses, confirm that the following items are present in the figure legend, table legend, main text, or Methods section.

n/a Confirmed

- |                                     |                                     |  |
|-------------------------------------|-------------------------------------|--|
| <input type="checkbox"/>            | <input checked="" type="checkbox"/> | The exact sample size ( $n$ ) for each experimental group/condition, given as a discrete number and unit of measurement  |
| <input type="checkbox"/>            | <input checked="" type="checkbox"/> | A statement on whether measurements were taken from distinct samples or whether the same sample was measured repeatedly  |
| <input type="checkbox"/>            | <input checked="" type="checkbox"/> | The statistical test(s) used AND whether they are one- or two-sided<br><i>Only common tests should be described solely by name; describe more complex techniques in the Methods section.</i>   |
| <input checked="" type="checkbox"/> | <input type="checkbox"/>            | A description of all covariates tested   |
| <input type="checkbox"/>            | <input checked="" type="checkbox"/> | A description of any assumptions or corrections, such as tests of normality and adjustment for multiple comparisons  |
| <input type="checkbox"/>            | <input checked="" type="checkbox"/> | A full description of the statistical parameters including central tendency (e.g. means) or other basic estimates (e.g. regression coefficient) AND variation (e.g. standard deviation) or associated estimates of uncertainty (e.g. confidence intervals) |
| <input type="checkbox"/>            | <input checked="" type="checkbox"/> | For null hypothesis testing, the test statistic (e.g. $F$ , $t$ , $r$ ) with confidence intervals, effect sizes, degrees of freedom and $P$ value noted<br><i>Give <math>P</math> values as exact values whenever suitable.</i>                            |
| <input checked="" type="checkbox"/> | <input type="checkbox"/>            | For Bayesian analysis, information on the choice of priors and Markov chain Monte Carlo settings   |
| <input checked="" type="checkbox"/> | <input type="checkbox"/>            | For hierarchical and complex designs, identification of the appropriate level for tests and full reporting of outcomes   |
| <input checked="" type="checkbox"/> | <input type="checkbox"/>            | Estimates of effect sizes (e.g. Cohen's $d$ , Pearson's $r$ ), indicating how they were calculated   |

*Our web collection on [statistics for biologists](#) contains articles on many of the points above.*

### Software and code

Policy information about [availability of computer code](#)

Data collection	Scanford Custom FACSScan Analyzer, BD LSRII, BD Aria II software (flow cytometry). SpectraMax 190 and SpectraMax iD3 software (multi-mode microplate reader). Zen Black and Zen Blue (confocal microscopy); Leica Application Suite X software and NIS-Elements F software (light microscopy, immunohistochemistry and immunofluorescence). Hidex Automatic Gamma Counter software (gamma counter).
Data analysis	GraphPad Prism 7 (statistical analysis of the majority of in vitro and in vivo experiments). FlowJo10.1.r5 (flow cytometry). Adobe Photoshop CS6 and ImageJ version 1.52 (blinded histology). Inveon Research Workplace (PET/CT). Single-cell RNA sequencing data pre-processing (10x Cell Ranger v3.0.2) and downstream analyses (Seurat R package v3.0). PANTHER GO ontology database (version released 2019-01-01). GOplot (v1.0.2).

For manuscripts utilizing custom algorithms or software that are central to the research but not yet described in published literature, software must be made available to editors/reviewers. We strongly encourage code deposition in a community repository (e.g. GitHub). See the Nature Research [guidelines for submitting code & software](#) for further information.

### Data

Policy information about [availability of data](#)

All manuscripts must include a [data availability statement](#). This statement should provide the following information, where applicable:

- Accession codes, unique identifiers, or web links for publicly available datasets
- A list of figures that have associated raw data
- A description of any restrictions on data availability

The data that support the findings of this study are available from the corresponding author upon reasonable request.

## Field-specific reporting

Please select the one below that is the best fit for your research. If you are not sure, read the appropriate sections before making your selection.

- Life sciences     Behavioural & social sciences     Ecological, evolutionary & environmental sciences

For a reference copy of the document with all sections, see [nature.com/documents/nr-reporting-summary-flat.pdf](https://www.nature.com/documents/nr-reporting-summary-flat.pdf)

## Life sciences study design

All studies must disclose on these points even when the disclosure is negative.

Sample size	Sample sizes were determined based on prior extensive experience with mouse models of vascular disease. In atherosclerosis intervention studies, a minimum of 8-10 animals per sex per group was considered sufficient to detect changes that are biologically significant and is a common sample size in the field.
Data exclusions	No data was excluded.
Replication	All experiments were performed with biological replicates, and technical replicates were performed for studies as described in the Methods section, Figure Legends, and Main text. Experimental findings were reliably reproduced.
Randomization	Each animal was randomized into an experimental group at the time of study initiation.
Blinding	Investigators performing quantitative analysis of histology were blinded to the experimental group until all data had been collected.

## Reporting for specific materials, systems and methods

We require information from authors about some types of materials, experimental systems and methods used in many studies. Here, indicate whether each material, system or method listed is relevant to your study. If you are not sure if a list item applies to your research, read the appropriate section before selecting a response.

### Materials & experimental systems

n/a	Involved in the study
<input type="checkbox"/>	<input checked="" type="checkbox"/> Antibodies
<input type="checkbox"/>	<input checked="" type="checkbox"/> Eukaryotic cell lines
<input checked="" type="checkbox"/>	<input type="checkbox"/> Palaeontology
<input type="checkbox"/>	<input checked="" type="checkbox"/> Animals and other organisms
<input checked="" type="checkbox"/>	<input type="checkbox"/> Human research participants
<input checked="" type="checkbox"/>	<input type="checkbox"/> Clinical data

### Methods

n/a	Involved in the study
<input checked="" type="checkbox"/>	<input type="checkbox"/> ChIP-seq
<input type="checkbox"/>	<input checked="" type="checkbox"/> Flow cytometry
<input checked="" type="checkbox"/>	<input type="checkbox"/> MRI-based neuroimaging

## Antibodies

Antibodies used	Anti-CD47 antibodies (clone MIAP410, BioXcell, 10 ug/ml) and IgG1 control antibodies (clone MOPC-21, BioXcell, 10 ug/ml). Flow cytometry: anti-CD16/32 (clone 2.4G2, BD Biosciences, 553142, 3 ug per 10 <sup>6</sup> cells), Alexa Fluor 594-anti-Vimentin (clone EPR3776, Abcam, ab154207, 1:50), APC-anti-CD31 (clone 390, Invitrogen, 17-0311-80, 1:50), FITC-anti-Ly-6C (clone AL-21, BD Biosciences, 553104, 1:100), PE-Cy5-labeled anti-CD5 (clone 53-7.3, BioLegend, 100609, 1:50), PE-Cy7-anti-Gr-1 (clone RB6-8C5, Invitrogen, 25-5931-81, 1:50), APC-Cy7-anti-CD11b (clone M1/70, BioLegend, 101225, 1:50), Pacific Blue-anti-F4/80 (clone BM8, BioLegend, 123123, 1:100), FITC-anti-CD11b (clone M1/70, Invitrogen 11-0112-81, 1:100), and Alexa Fluor 488-anti-alpha-smooth muscle actin (clone 1A4, eBioscience, 50-112-4644, 1:100). Immunohistochemistry/Immunofluorescence: Phospho-SHP1 (Abcam, ab131500, 1:50), Mac-3 (BD Sciences, BD 550292, 1:100), cleaved caspase-3 (Cell Signaling, 9661, 1:200), and anti-PEG (Abcam, PEG-B-47, ab51257, 1:100).
Validation	Anti-CD47 antibodies (clone MIAP410, BioXcell) and IgG1 control antibodies (clone MOPC-21, BioXcell); species reactivity tested and validated by the manufacturer and in reference: CD47-blocking antibodies restore phagocytosis and prevent atherosclerosis, doi: 10.1038/nature18935. Per data sheet anti-CD16/32 (clone 2.4G2, BD Biosciences, 553142) is referenced in 18 publications; per data sheet Alexa Fluor 594-anti-Vimentin (clone EPR3776, Abcam, ab154207) is referenced in 5 publications; per data sheet APC-anti-CD31 (clone 390, Invitrogen, 17-0311-80) is referenced in 40 publications; per data sheet FITC-anti-Ly-6C (clone AL-21, BD Biosciences, 553104) is referenced in 7 publications; per data sheet PE-Cy5-labeled anti-CD5 (clone 53-7.3, BioLegend, 100609) is referenced in 5 publications; per data sheet PE-Cy7-anti-Gr-1 (clone RB6-8C5, Invitrogen, 25-5931-81) is referenced in 8 publications; per data sheet APC-Cy7-anti-CD11b (clone M1/70, BioLegend, 101225) is referenced in 60 publications; per data sheet Pacific Blue-anti-F4/80 (clone BM8, BioLegend, 123123) is referenced in 21 publications; per data sheet FITC-anti-CD11b (clone M1/70, Invitrogen 11-0112-81) is referenced in 240 publications; per data sheet Alexa Fluor 488-anti-alpha-smooth muscle actin (clone 1A4, eBioscience, 50-112-4644) is referenced in 2 publications. Phospho-SHP1 (Abcam, ab131500), Mac-3 (BD Sciences, BD 550292), cleaved caspase-3 (Cell Signaling, 9661); species reactivity tested and validated by the manufacturer

and in reference: CD47-blocking antibodies restore phagocytosis and prevent atherosclerosis, doi: 10.1038/nature18935. Anti-PEG (Abcam, PEG-B-47, ab51257); reactivity tested and validated by the manufacturer and is referenced in 42 publications.

## Eukaryotic cell lines

Policy information about [cell lines](#)

Cell line source(s)	Human monocyte cells (THP-1, ATCC TIB-202), mouse macrophage cells (RAW264.7, ATCC TIB-71), and mouse yolk sac endothelial cells (C166, ATCC CRL-2581) were purchased from American Type Culture Collection (ATCC). Human coronary artery smooth muscle cells (HCASMCs, Lonza CC-2583) and human aortic endothelial cells (HAECs, Lonza CC-2535) were purchased from Lonza. The cell lines were not validated.
Authentication	Cell lines are tested and authenticated by ATCC or Lonza in a systematic process including morphology assessment, karyotyping, and PCR-based approaches. Following receipt from ATCC or Lonza, the identity of the cell lines were confirmed through assessment of cellular morphology under microscope.
Mycoplasma contamination	Lonza: HIV-1, hepatitis B and hepatitis C are not detected for all donors and/or cell lots. All cells are performance assayed and test negative mycoplasma, bacteria, yeast and fungi. ATCC: mycobacterium negative; bacterium and yeast negative; HIV-1, hepatitis B and hepatitis C negative.
Commonly misidentified lines (See <a href="#">ICLAC</a> register)	No commonly misidentified cell lines were used.

## Animals and other organisms

Policy information about [studies involving animals](#); [ARRIVE guidelines](#) recommended for reporting animal research

Laboratory animals	Apolipoprotein-E-deficient (apoE <sup>-/-</sup> ) mice on a C57BL/6 background were purchased from the Jackson laboratory. Both male and female animals were used. Mice were used at 20-24 weeks of age for biodistribution studies, and 8-10 weeks of age for atherosclerosis intervention studies.
Wild animals	The study did not involve wild animals.
Field-collected samples	The study did not involve samples collected from the field.
Ethics oversight	The study protocol was approved by the Stanford University IACUC and Administrative Panel on Laboratory Animal Care (protocol 27279).

Note that full information on the approval of the study protocol must also be provided in the manuscript.

## Flow Cytometry

### Plots

Confirm that:

- The axis labels state the marker and fluorochrome used (e.g. CD4-FITC).
- The axis scales are clearly visible. Include numbers along axes only for bottom left plot of group (a 'group' is an analysis of identical markers).
- All plots are contour plots with outliers or pseudocolor plots.
- A numerical value for number of cells or percentage (with statistics) is provided.

### Methodology

Sample preparation	Unchecked box above is not applicable to certain data presented in the manuscript. Sections in the Methods (SWNT in vitro uptake assay, efferocytosis assay, plaque targeting and biodistribution, SWNT cellular uptake profile, aortic single cell preparation for single-cell RNA sequencing) contain details of sample preparation, including isolation of single cell suspensions and staining protocols.
Instrument	The Scanford Custom FACSScan Analyzer was used for in vitro uptake and phagocytosis assays. The BD LSR II and BD Aria II was used for in vivo cellular uptake profiling and sorting of cells for single-cell RNA sequencing.
Software	FlowJo10.1.r5 (Tree Star, Inc.)
Cell population abundance	Post-sort fractions included >75,000 cells or events per sample. Cells were then counted using C-chip hemacytometers and in adherence to the Chromium Single Cell 3' Reagent Kits v2 User Guide, each sample was re-suspended to a final cell stock concentration of 600-1,000 cells per microliter.

Gating strategy

Cells were first gated to exclude debris (using FSC-A vs. SSC-A, or FSC vs. SSC), followed by gating for singlets (using FSC-W vs. FSC-A, or FSC vs. FSC-W) and then viable cells (using the SYTOX Blue Dead Cell stain). Gates were set for Cy5.5-positive vs. Cy5.5-negative cells using samples from PBS-treated controls.

Tick this box to confirm that a figure exemplifying the gating strategy is provided in the Supplementary Information.